SOURCE TERM THRUST

Rodney C. Ewing[1] and Mark T. Peters[2]
Source Term Thrust

[1]University of Michigan | [2]Argonne National Laboratory (ANL)
Contact: Rod Ewing: rodewing@umich.edu
Mark Peters: mtpeters@anl.gov

The goal of the Source Term Thrust is to enhance the understanding of the performance of nuclear waste forms (mainly spent nuclear fuel [SNF] and nuclear waste glass) and to quantify the release of radionuclides in the evolving near-field environment expected at the proposed nuclear waste repository at Yucca Mountain, Nevada. The behavior of the source term, mainly SNF and vitrified waste, limits radionuclide releases, both initially and over the long term. Interactions of the source term with the near-field environment, such as corroded waste packages, place additional constraints on the long-term behavior, including retention and mobility of important radionuclides.

This program is directed at developing a basic understanding of the fundamental mechanisms of radionuclide release and a quantification of the release as repository conditions evolve over time, particularly at longer times (>100,000 years). Radionuclide release will be critically sensitive to variations in temperature, radiation field, redox conditions, pH, pCO_2, surface area-to-solution volume, and presence of near-field materials. Among the important processes that can control radionuclide release are: (1) kinetics of waste form corrosion, (2) formation of secondary, alteration phases, and (3) reduction and sorption onto the surfaces of near-field materials.

Predictions of the long-term behavior of nuclear waste forms cannot be based entirely on models of laboratory results that are then extrapolated to long periods. Hence, this program will integrate multiple lines of evidence (e.g., results from natural analogue studies) to clarify the scientific basis for waste-form-degradation mechanisms in relation to source term models. The program will evaluate the uncertainties introduced by parametric uncertainty, variations in environmental conditions, and the use of different conceptual models.

The present source term and near-field models in the Yucca Mountain performance assessment are conservative, but the uncertainties are large. To the extent that the mechanisms of release for specific radionuclides can be understood or the uncertainties decreased, the subsequent analysis of the far-field barriers becomes less important. In the present performance assessment, important processes that will certainly occur are not explicitly included, such as the formation of secondary, U^{6+} alteration phases. Very little credit is taken for the potential chemical interactions between released radionuclides and the alteration products of the SNF and metal waste packages, or their internal components. The conservatism of the present models may be reduced by an improved understanding of the fundamental geochemical/hydrologic processes that will control the corrosion of SNF under oxidizing conditions and the potential interactions that may occur among the corroded nuclear fuel, the high-level-waste (HLW)-borosilicate glass, and the waste package components. This focused and integrated research program will provide the scientific basis for the development of the next generation of more realistic models for source term and near-field processes. Although there has been considerable research on the corrosion of SNF and nuclear waste glasses, there has been much less work on developing models that are applicable to an oxidizing environment, such as that at the proposed Yucca Mountain repository.

There are two compelling reasons for the importance of understanding the source term and near-field behavior. First, essentially all radioactivity is initially in the waste form, mainly SNF or nuclear waste glass. An enhanced understanding and realistic estimates of the extent to which radionuclides will be retained in the waste form or near-field environment reduce demands on the performance of subsequent, far-field barriers. Realistic estimates of radionuclide release can also reduce uncertainties in the Total System Performance Assessment. Second, over long periods, as engineered barriers degrade, it is the waste forms that eventually provide the release of radioactivity to the environment. Thus, it is essential to predict with confidence the physical and chemical evolution of the waste form over hundreds of thousands of years.

Finally, the need to understand the corrosion and alteration of SNF and nuclear waste glasses is a research subject unique to the needs of the Office of Civilian Radioactive Waste Management (OCRWM) Science and Technology program. Other agencies and DOE offices, such as the National Science Foundation (NSF) or Office of Basic Energy Sciences (OBES), generally do not fund research on the properties or corrosion of SNF or nuclear waste glasses. Hence, OCRWM, by supporting this program, is creating a community of scientists and engineers who are actively working on and knowledgeable in this field. An important component of this program is the connection to international efforts, particularly to the European Community (EC) programs. We are in the process of connecting our research program to NF-Pro, a four-year integrated project (2004–2007) supported by the EC, as part of their Sixth Framework Program. NF-Pro brings together 40 nuclear research and waste management organizations

with the aim of integrating European research on the near field. We have also initiated contact with the EU MICADO (Model uncertainty for the mechanism of dissolution of spent fuel in a nuclear waste repository) program. Through these collaborations, we will leverage present U.S. funding for increased understanding and enhance the international knowledge and reputation of the U.S. program.

The present program, summarized in the following pages, consists of 15 separate programs that involve five national laboratories and five universities (one in Great Britain). In many instances, university investigators have programs closely tied to national laboratories in order to utilize unique facilities for handling highly radioactive materials. Three of the graduate students in this program are supported by OCRWM Fellowships and have completed practica at national laboratories this past summer.

The research programs address four critical areas:

SNF Dissolution Mechanisms and Rates

The initial release of radionuclides is governed by the specific mechanisms and rates of dissolution, which in turn, vary as a function of pH, dissolved oxygen concentration, temperature, solution composition, fuel chemistry (i.e., burn-up), and mode of contact with water. Systematic studies are being conducted of radionuclide release from SNF as a function of these parameters, with special attention being paid to the effects of radiolysis on matrix dissolution rates and the formation of secondary phases. The program also investigates the effects of water that may condense and accumulate on failed SNF pins. By the process of deliquescence of hygroscopic fission product phases, alteration products may form on the surfaces of the SNF.

Descriptions of this individual program area are provided in the two-page summaries on pp. 9–16.

Formation and Properties of U^{6+} Secondary Phases

Under an oxidizing environment, the corrosion of SNF leads to the formation of a complicated array of U^{6+} secondary phases that may retard release of radionuclides either by co-precipitation/incorporation, sorption, or by forming a physical barrier to the continued contact with water or release of radionuclides. We have established a multi-pronged approach that includes carefully controlled experiments to determine the means and extent of radionuclide incorporation (e.g., ^{237}Np, ^{239}Pu, and ^{129}I) and sorption into and onto the structures of U^{6+} secondary phases. The experimental work is supported by the application of advanced techniques (x-ray absorption spectroscopy at the Advanced Photon Source at Argonne

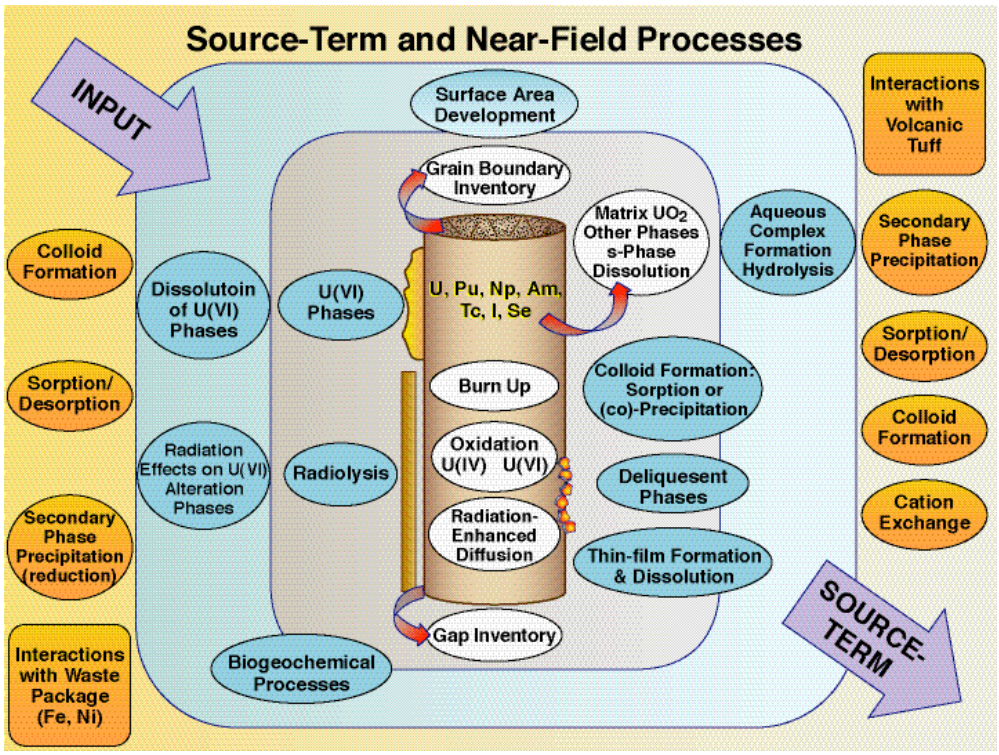

Schematic illustration of the potentially important processes in the Source Term Thrust research program.

National Laboratory, laser-ablation inductively coupled plasma mass spectroscopy, and *in situ* spectroelectrochemical techniques) in order to determine the extent of incorporation and sorption of radionuclides in/on U^{6+}- secondary phases. The stability of these phases is being determined by high-temperature oxide-melt solution calorimetry and reversible solubility measurements, as well as systematic irradiation experiments. Computational simulations involving quantum mechanical calculations are being used to investigate the energetics of the incorporation and sorption processes. In addition, actinide complex stability constants at elevated temperatures are being measured using potentiometry, solvent extraction, spectrophotometric, and nuclear magnetic resonance measurements. The experimental and modeling studies are supported and confirmed by studies of natural occurrences of SNF, namely at the Oklo natural reactors.

Descriptions of this individual program area are provided in the two-page summaries on pp. 17–37.

Waste Form–Waste Package Interactions in the Near Field

The SNF will corrode and release radionuclides in an environment dominated by the presence of uranium, iron, and solutions whose compositions are the result of interactions with the waste forms, waste packages, and the surrounding volcanic tuff. These interactions buffer the environment in which the SNF corrodes and also offer additional opportunities for reduced mobility of radionuclides. We have research programs to investigate the types and behaviors of waste package corrosion products, and their potential for reduction and sorption of key radionuclides (e.g., uptake of ^{99}Tc onto iron oxyhydroxides). We also will investigate the interactions of UO_2 with solutions in contact with volcanic tuff using the pressurized unsaturated flow (PUF) system and *in situ* analytical techniques to investigate and characterize the secondary phases that form. Again, computational simulations of atomic-scale interactions will be used to interpret and support the experimental results.

Descriptions of this individual program area are provided in the two-page summaries on pp. 39–46.

Integration of In-Package Chemical and Physical Processes

The greatest challenge for this program is to integrate the scientific results into a larger scale model of the source term and near-field interactions. To accomplish this, we have immediately begun creating numerical models that capture the important physical and chemical processes that lead to radionuclide release from SNF. The source term model will be coupled to a drift/near-field-scale model that captures the relevant thermal-hydrologic-chemical regimes as a function of time. This integrated model will be used to establish the scientific links among our science programs and provide a basis for understanding the behavior of SNF at different time frames: (1) prior to breach of the waste package; (2) at the time of early breaches of the waste package at elevated temperature; and (3) after breach at long periods, greater than 100,000 years, but at essentially ambient conditions.

Descriptions of this individual program area are provided in the two-page summaries on pp. 47–52.

This page intentionally left blank.

SNF Dissolution Mechanisms and Rates

Actinide Thermodynamics at Elevated Temperatures
Judah Friese, Yuanxian Xia, and Paula P. Bachelor, Pacific Northwest National Laboratory (PNNL)
Linfeng Rao and Guoxin Tian, Lawrence Berkeley National Laboratory (LBNL)

Dissolution Mechanisms and Rates
Amanda Kline and William Miller, University of Missouri-Columbia
Brady Hanson, Pacific Northwest National Laboratory (PNNL);

Implications of Deliquescence and Decay Heat on Source Term Degradation
James Jerden, Argonne National Laboratory (ANL)

This page intentionally left blank.

Actinide Thermodynamics at Elevated Temperatures

Judah Friese [1], Linfeng Rao[2], Yuanxian Xia[1], Paula P. Bachelor[1], and Guoxin Tian[2]

[1]Pacific Northwest National Laboratory (PNNL) | [2]Lawrence Berkeley National Laboratory (LBNL)

Research Objectives

The postclosure chemical environment in the proposed Yucca Mountain repository is expected to experience elevated temperatures. Predicting potential migration of actinides would be more robust if sufficient reliable thermodynamic data on hydrolysis and complexation are available for these temperatures. Data are scarce and scattered for 25°C, and nonexistent for elevated temperatures. Current modeling of actinide migration makes conservative assumptions to compensate for this lack of data, particularly at elevated temperatures.

This collaborative project between LBNL and PNNL collects thermodynamic data at elevated temperatures on actinide complexes with inorganic ligands that may be present in Yucca Mountain. The ligands include hydroxide, fluoride, sulfate, phosphate, and carbonate. Thermodynamic parameters of complexation, including stability constants, enthalpy, entropy, and heat capacity of complexation, are measured with a variety of techniques, including solvent extraction, potentiometry, spectrophotometry, and calorimetry.

Approach

Acid-base potentiometry measures electromotive force (*emf*) as a function of the concentration of hydrogen ion that in turn depends on reactions in solution, including ligand protonation and metal complexation. Thus, the measured *emf* can be used to calculate the stability constants of actinide complexes. Solvent extraction uses the change of distribution coefficients with the ligand concentration to determine metal complexation stability constants. With spectrophotometric methods, the oxidation states and nature of actinide species are identified by characteristic absorption bands (e.g., Np(V) at 980 nm and Pu(VI) at 830 nm). From the change of absorbance as a function of concentrations of reagents, the stability constants of actinide complexes are determined. Nuclear magnetic resonance (NMR) spectroscopy measures chemical shifts in species of nuclei present according to fractional populations. Since the magnitude of chemical shifts depends on the values of the equilibrium constant, the chemical shift becomes a function determined analogous to the potentiometric case.

Titration calorimetry directly measures reaction heat released (or absorbed) when a solution is titrated with a titrant. Since the reaction heat in a complexation titration is a function of the concentrations of reagents, the stability constant(s) of complex(es), and the enthalpy of complexation, the latter can be calculated from calorimetric titrations.

Accomplishments

Complexation of Pu(IV) and Pu(VI) at Elevated Temperatures

Thermodynamic studies of actinide complexation at elevated temperatures were extended from uranium and neptunium to plutonium, another important transuranic element of great concern in environmental transport. Complexation of Pu(IV) with F^- was studied at 25–55°C by solvent extraction (Figure 1). The equilibrium constants of the reactions, $Pu^{4+} + iHF = PuF_i^{(4-i)+} + iH^+$ where i = 1 and 2, were found to decrease with increasing temperature.

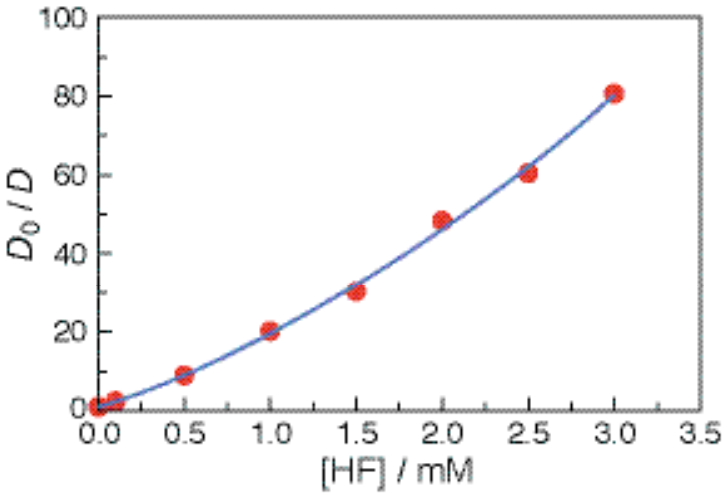

Figure 1. Solvent extraction of Pu(IV) in the presence of HF: Plot of D_0/D vs. [HF], solid symbol—experimental, curve—calculated. Aqueous phase—Pu(IV) in 2.0 M $HClO_4$ + HF; organic phase—0.05 M TTA in toluene; t = 55°C.

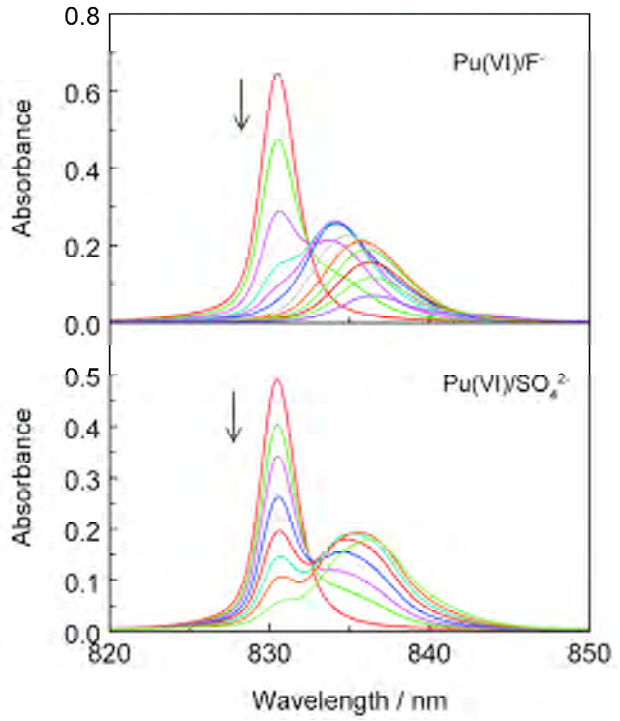

Figure 2. Spectrophotometric titration of Pu(VI) complexation with fluoride and sulfate (I = 1.0 M $NaClO_4$, t = 25°C, optical path = 1.00 cm). Top—Pu(VI)/fluoride: V^0 = 2.50 mL, C_{Pu}^0 = 1.18 x 10^{-3} M, C_H^0 = 1.51 x 10^{-3} M; titrant: 1.00 M NaF, 3.29 mL added. Bottom—Pu(VI)/sulfate: V^0 = 2.50 mL, C_{Pu}^0 = 8.93 x 10^{-4} M, C_H^0 = 1.14 x 10^{-3} M; titrant: 0.50 M Na_2SO_4, 1.50 mL added.

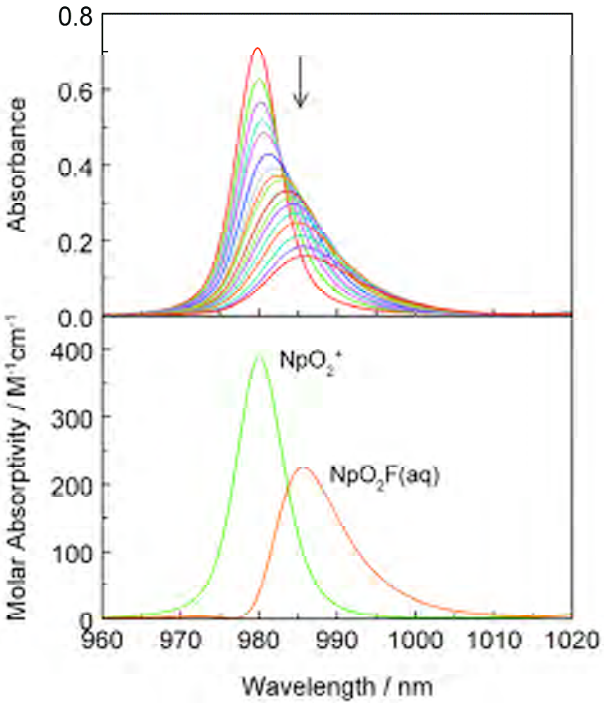

Figure 3. Spectrophotometric titration of Np(V) fluoride complexation (I = 1.0 M $NaClO_4$, t = 25°C, optical path = 1.00 cm). Top—17 spectra, V^0 = 2.50 mL, C_{Np}^0 = 1.82 ? 10^{-3} M, C_H^0 = 1.0 ? 10^{-6} M; titrant: 1.00 M NaF, a total of 2.40 mL added in 16 additions. Bottom—calculated molar absorptivities of Np(V) species.

Complexation of Pu(VI) with F^- and SO_4^{2-} was studied at 25°C by spectrophotometry using the characteristic absorption band of Pu(VI) at 830 nm (Figure 2). Calculations of stability constants are in progress.

Spectrophotometric Measurements on Np(V) and U(VI) at Elevated Temperatures

Spectrophotometric titrations were performed to measure the stability constants of U(VI)/F^-, U(VI)/SO_4^{2-}, Np(V)/F^- and Np(V)/SO_4^{2-} complexes at 25–70°C (Figure 3). It was found that all these complexes become stronger at higher temperatures.

Microcalorimetric Measurements on Np(V) and Pu(VI)

Calorimetric titrations of Np(V)/F^- and Np(V)/SO_4^{2-} complexes were completed, and data processing with new stability constants obtained by spectrophotometry is in progress. A representative calorimetric titration is shown in Figure 4. Calorimetric titrations of Pu(VI) systems have been started.

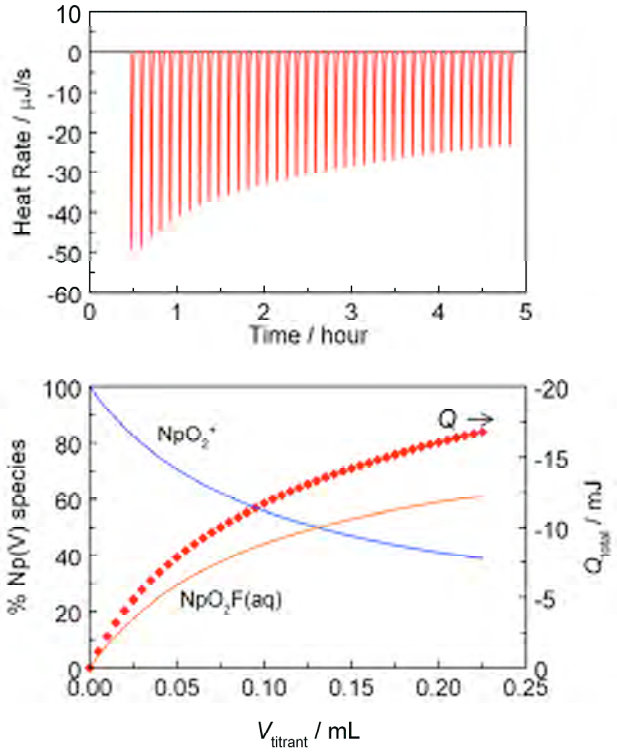

Figure 4. Calorimetric titration of Np(V) fluoride complexation (I = 1.0 M $NaClO_4$, t = 25°C). V^0 = 0.900 mL, C_{Np}^0 = 1.78 x 10^{-3} M, C_H^0 = 3.0 x 10^{-7} M; titrant: 1.0 M NaF, 5 microL/addition.

Dissolution Mechanisms and Rates

Amanda Kline[1], Brady Hanson[2], and William Miller[1]
[1]University of Missouri-Columbia | [2]Pacific Northwest National Laboratory (PNNL)

Research Objectives

This research focuses on the examination of the variables associated with spent nuclear fuel (SNF) dissolution. The project consists of both theoretical and experimental techniques in order to achieve a better understanding of parameters affecting dissolution, such as temperature, dissolved O_2 concentrations, flow rates, fuel chemistry, and radiolysis of the solution in contact with the fuel.

Approach

The rate of dissolution of SNF is dependent upon many factors, and the extent to which each variable affects the dissolution rate varies greatly. Recently, the effect of radiolysis on fuel dissolution has become the focus of international attention. However, most of this attention is on how radiolysis alters otherwise reducing environments. Since radiolysis produces radicals and molecules (e.g., H_2O_2) that are more oxidizing than dissolved oxygen, the effects of radiolysis even under oxidizing conditions may be significant. Modeling is used to calculate the radiation dose to water from SNF, allowing a more accurate depiction of the water chemistry in contact with the fuel. Experimental work utilizing single-pass flowthrough (SPFT) tests were used to determine the dependence of the dissolution rate on each parameter and to validate the models.

The primary objective of our research is to determine the effect β- and γ-radiolysis has on SNF dissolution rates, especially when determining their contribution to the dissolution rate on fresh (i.e., <30 years old) SNF, as has been performed in support of geologic disposal. The effect of each type of radiation on water radiolysis and subsequent fuel dissolution will be examined by preparing sintered UO_2 pellets doped with single radionuclides and testing the specimens using SPFT. Non-uranium dopants, such as fission products and actinides, that alter the fuel chemistry and dissolution rates must also be examined, so that fuel chemistry and radiolysis effects can be determined separately. The chemistry effect can be determined using the same fuel preparation and SPFT techniques, but utilizing nonradioactive isotopes.

Accomplishments

Two models have been developed and presented to determine the effects of radiolysis on SNF dissolution. First, a systematic dosimetry model to determine the dose to water from SNF was developed (Miller et al., 2006). MCNP5 and a random-walk Monte Carlo model implemented in Mathematica were used to calculate the dose as a function of parameters such as radiation type and energy, distance from the fuel, fuel particle size (e.g., surface-to-volume ratio) and fuel-to-water ratios. The second model (Kline et al., 2006) uses the dose obtained by the first model for SNF of specific burnup and decay time. A Fortran code and the simultaneous differential equation solver ODEPACK were used in the second model to calculate the concentrations of species that make up the water chemistry, by first determining the initial radiolytic yields, as determined by the G-values, and then solving 129 simultaneous reactions for the 32 species included. Figure 1 shows the large effect of radiation dose on the concentration of the main oxidizers by comparing the model results from 23-year-old SNF to those surrounding unirradiated UO_2 in an oxidizing environment without any bicarbonate in solution. H_2O_2 shows approximately a 4-order-of-magnitude increase, and O_2- and OH each show approximately a 2-order-of-magnitude increase for SNF.

Dissolution rates are being measured using SPFT, where the flow rate is sufficiently high to minimize back reactions and to maintain the uranium concentration well below solubility limits, in order to prevent alteration phase formation. The

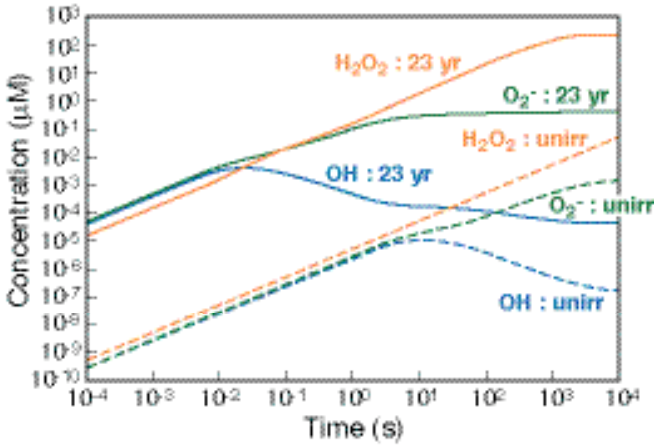

Figure 1. Comparison of the predicted concentration of main oxidizers contacting unirradiated UO_2 and 23-year-old SNF.

system has been designed to maintain a well-mixed solution equilibrated at operating temperature, with a sparge gas containing 20.9% O_2 and enough CO_2 to maintain a total carbonate concentration of 2×10^{-3} M and constant pH. The pre-equilibration at temperature is an important design feature by which to precisely control dissolved oxygen concentrations and minimize effects of exsolved oxygen. At 25°C, 50°C, and 75°C, the dissolved oxygen concentrations are 8.7 ppm, 5.9 ppm, and 4.2 ppm, respectively. Dissolved oxygen concentrations and pH are measured continuously with on-line sensors. The fuels used for the initial tests are from reactor-grade pellets procured from a commercial vendor. SPFT tests on two fuels, one being natural enriched UO_2 and the second being 4.6% enriched UO_2 containing 8 wt% Gd, are ongoing (Kline et al., 2007). Figure 2 shows the results from the tests on these two fuels, each conducted at three different flow rates.

Based on the model results, one would expect the dissolution rate of fresh SNF to be significantly higher than for unirradiated UO_2, due to the increased concentration of radiolytically-produced highly oxidizing species. Over the first 500 years after irradiation, the contribution of β and γ radiation decreases by approximately four orders of magnitude (Miller et al., 2006). The long-term radiolysis contribution will be from α decay of long-lived actinides. This suggests that the dissolution rates reported on fresh SNF are significantly higher than they will be for aged fuel under repository conditions. Similarly, the results on doped fuels suggest that in the absence of the radiolytic field, SNF will have smaller dissolution rates than unirradiated UO_2 as a result of the changes in fuel chemistry. Both the reduction in radiolysis effect over time and the chemical stabilization effect are expected to show that current dissolution rates for both fresh SNF and unirradiated UO_2 are higher than the long-term dissolution rates will be for SNF under geologic conditions. Initial results such as in Figure 2 suggest that the dependence on dissolved oxygen may be underestimated and the temperature dependence overestimated in current models, owing to exsolved oxygen issues.

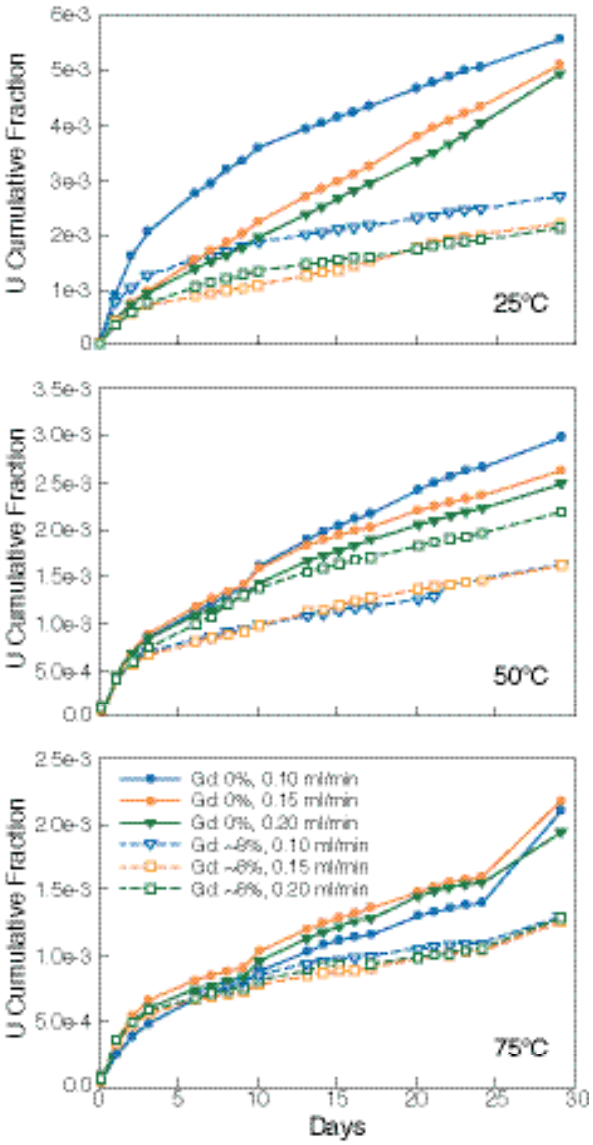

Figure 2. Results from SPFT tests on UO_2 and 8wt% Gd-doped UO_2 at 25°C, 50°C, and 75°C at 0.1, 0.15 and 0.2 mL min^{-1}.

The work of Amanda Kline was performed under appointment of the Office of Civilian Radioactive Waste Management Fellowship Program administered by Oak Ridge Institute for Science and Education under a contract between the U.S. Department of Energy and the Oak Ridge Associated Universities.

Related Publications

Miller, W., A. Kline, and B. Hanson, Dosimetry modeling at the fuel-water interface. Proceedings of the 11th International High-Level Radioactive Waste Management Conference (IHLRWM), American Nuclear Society, Las Vegas NV, pp. 698–711, 2006.

Kline, A., B. Hanson, W. Miller, and R. Wittman, Modeling the radiolysis effect on CSNF dissolution kinetics. Transactions of the American Nuclear Society Winter Meeting, 95, 177–178, Albuquerque, New Mexico, 2006.

Kline, A., B. Hanson, and W. Miller, Characteristics of UO_2 dissolution as determined by SPFT Tests. American Nuclear Society Winter Meeting 2007 (submitted).

Implications of Deliquescence and Decay Heat on Source Term Degradation

James Jerden
Argonne National Laboratory (ANL)

Research Objectives

The goal of this project was to quantify processes that could cause water to condense and accumulate on failed spent nuclear fuel (SNF) pins. A particularly important process in this regard is the deliquescence of hygroscopic fission product minerals present within fuel grain boundaries and the fuel/cladding gap. Deliquescence could lead to the accumulation of water, despite the fact that the fuel assemblies will be the hottest material in the waste packages. The specific experimental objectives were to: (1) develop a predictive understanding of the onset of deliquescence on SNF by quantifying the deliquescence thresholds (as a function of temperature) of hygroscopic primary phases in the fuel or fuel/cladding gap, (2) develop a predictive understanding of how the aqueous films that form from deliquescence evolve chemically as the SNF corrodes at relevant temperatures and relative humidities, (3) determine the paragenesis, mineral chemistry, and deliquescence behavior of alteration phases that form as SNF corrodes in aqueous films formed by deliquescence.

Approach

The deliquescence behavior of key fission-product salts has been quantified using an isopiestic method. This approach was based on the fact that in a closed system—consisting of a hygroscopic salt, an aqueous salt solution, and a gas phase—water will partition via evaporation or condensation until its chemical potential is equal in all phases. Our experiments involved reacting a dry powder of the hygroscopic mineral(s) of interest, with air of a known relative humidity at a

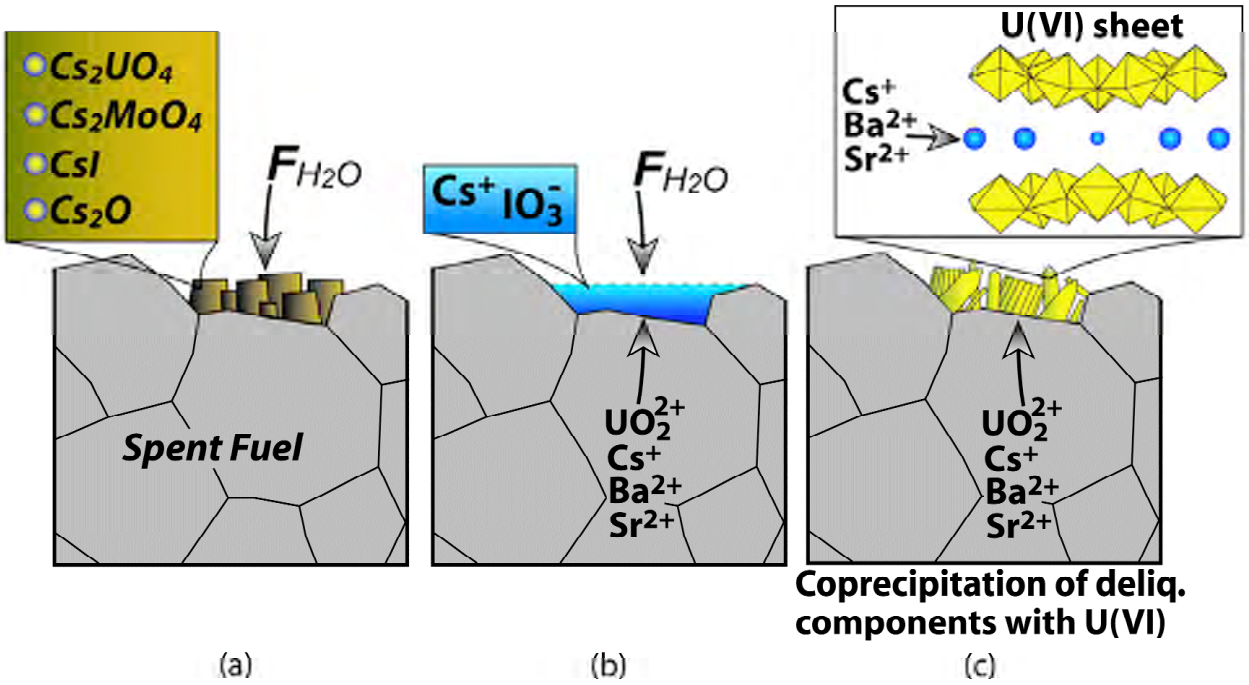

Figure 1. A summary of the processes involved in fission-product mineral deliquescence: (a) If the ambient relative humidity increases above approximately 80%, deliquescence will occur despite the fact that the fuel is 1°C–5°C hotter than the surrounding environment; (b) water will continue to condense as long as the activity of water in the deliquescent brine is lower than the ambient relative humidity; (c) the precipitation of uranyl corrosion phases counteracts deliquescence (increases the activity of water in the deliquescent brine) as deliquescent components are incorporated into the nondeliquescent uranyl minerals. Thus, the precipitation of uranyl minerals promotes evaporation of water from the SNF surface.

controlled temperature in a sealed system. The initial relative humidity was controlled using a sodium chloride salt solution. When the deliquescence threshold (relative humidity at which water will condense) of the sample is exceeded, the amount of water that accumulates due to deliquescence was measured gravimetrically. The amount of water that accumulates as the deliquescent solution equilibrates with the surrounding gas phase was also measured gravimetrically.

Accomplishments

The deliquescence behavior of the hygroscopic fission product minerals cesium iodide (CsI), cesium molybdate (Cs_2MoO_4) and selected cesium uranates (Cs_2UO_4 and $Cs_2U_2O_7$) have been studied over temperatures ranging from 40°C to 90°C. We have also completed experiments investigating how the deliquescence process, and subsequent chemical evolution of brines, is influenced by SNF corrosion. These were performed by reacting SNF surrogates (uranium oxides) containing hygroscopic fission product minerals ($Cs_2UO_4 \pm Cs_2U_2O_7 \pm CsI \pm Cs_2MoO_4$) with humid air in a sealed isopiestic apparatus. Our experimental results have been used to quantify the conditions under which deliquescence could initiate SNF corrosion and how corrosion reactions may counteract deliquescent water accumulation.

Results indicate that fission product deposits containing cesium iodide, cesium molybdate, and the cesium uranate Cs_2UO_4 will deliquesce at relative humidities greater than 80% and temperatures ranging from 40°C to 90°C. This process will occur even if the SNF is up to 5°C hotter than the surrounding environment. Once the deliquescence process has started, water will continue to condense on the surface of the fuel as long as the activity of water in the brine is lower than the ambient relative humidity. However, our results also show that once SNF corrosion phases (uranyl minerals) begin to form, the deliquescence process becomes self-limiting, owing to the incorporation of deliquescent components into these stable alteration phases. The paragenesis of the alteration products is important in the sequestration of deliquescent components. Results from the SNF surrogate tests suggest that nondeliquescent uranyl minerals such as Cs-compreignacite [$(Cs_6[(UO_2)_{12}(OH)_{10}O_{10}](H_2O)_{3.5})$] and billietite [$(Ba)(UO_2)_6O_4(OH)_6(H_2O)_8$] play key roles in increasing the activity of water in the brine formed by deliquescence by sequestering barium and cesium. There was also evidence that iodine released from the deliquescence of CsI may be sequestered by the formation of other nondeliquescent uranyl iodate minerals of the general type $M(II)[(UO_2)_2(IO_3)_2O_2](H_2O)$ or $M(I)_2[(UO_2)_3(IO_3)_4O_2]$. The key finding of this project was that, while deliquescence may lead to a transient accumulation of water and incipient corrosion of SNF, this process will be counteracted (effectively "turned-off") by the sequestration of deliquescent components into nondeliquescent minerals (Figure 1).

Related Publications

Jerden, J.L. Jr., M. Goldberg, J. Cunnane, T. Bauer, R. Wigeland, and R. Nietert, Can spent nuclear fuel decay heat prevent radionuclide release? In: Scientific Basis for Nuclear Waste Management XXVIII, J.M. Hanchar, S. Stroes-Gascoyne, and L. Browning, eds., Materials Research Society Symposium Proceedings, 824, pp.101–106, Warrendale, PA, 2004.

Formation and Properties of U^{6+} Secondary Phases

Mitigation of the Release of ^{129}I from Spent Nuclear Fuel via Uptake by Uranyl Alteration Phases
Thomas E. Albrecht-Schmitt, Auburn University; Iain May, The University of Manchester, Great Britain

Impact of Uranyl Alteration Phases of Spent Fuel on Mobility of Neptunium (Np) and Plutonium (Pu) in Yucca Mountain
Peter C. Burns, University of Notre Dame

Actinide Adsorption to U(VI) Silicates
S. B. Clark, Washington State University; Lawrence C. Hull, Idaho National Laboratory

Corrosion of Spent Nuclear Fuel: The Long-Term Assessment
Rodney C. Ewing, University of Michigan

Direct Determination of the Thermodynamic Properties of Uranyl Minerals Important for the Performance of the Proposed Geological Repository at Yucca Mountain
Jeremy B. Fein, Peter C. Burns, University of Notre Dame; Alexandra Navrotsky, University of California, Davis

Chemical and Coordination Structure of Radionuclides in Spent Nuclear Fuel and Its Alteration Products: Understanding Release Pathways
Jeffrey A. Fortner, A. Jeremy Kropf, and James C. Cunnane, Argonne National Laboratory (ANL)

An *In Situ* Spectroelectrochemical Study of Neptunium (Np) Redox, Dissolution, and Precipitation Behavior at the Corroding Spent Nuclear Fuel/Alteration Phase Interface
Artem Guelis, Jeremy Kropf, Christopher Johnson, and Jeffrey Fortner, Argonne National Laboratory (ANL); Petr Vanysek, Northern Illinois University

Natural Sequestration of Radionuclides In Volcanic Tuff
Jonathan Icenhower, Edgar Buck, Eric Pierce, and Dawn Wellman, Pacific Northwest National Laboratory (PNNL); Andreas Lüttge, Rice University

Surface Charge and Radionuclide Adsorption Characteristics of U(IV,VI) Oxyhydroxides at 25–150°C
David J. Wesolowski, Laetitia Delmau, Lawrence M. Anovitz, Jorgen Rosenqvist, and Donald A. Palmer, Oak Ridge National Laboratory (ORNL)

This page intentionally left blank.

Mitigation of the Release of ^{129}I from Spent Nuclear Fuel via Uptake by Uranyl Alteration Phases

Thomas E. Albrecht-Schmitt[1] and Iain May[2]
[1]Auburn University | [2]The University of Manchester, Great Britain

Research Objectives

Iodine-129 (^{129}I) is a long-lived ($t_{1/2} = 1.7 \times 10^7$) β-emitting fission product present in spent nuclear fuel (SNF). In groundwater, such as that from the J-13 well near Yucca Mountain, it is expected to exist as both iodate, IO_3^-, and iodide. The objective of this program is to study the potential incorporation of $^{129}IO_3^-$ into uranyl alteration phases that will likely form as the result of the interaction of SNF with groundwater at the proposed repository in Yucca Mountain. We propose that the trigonal pyramidal iodate anion can substitute in trace amounts in the place of tetrahedral $[SiO_3(OH)]^{3-}$ and PO_4^{3-}, as well as for trigonal planar CO_3^{2-}. Experiments will be performed whereby uranyl silicates, phosphates, and carbonates are synthesized in the presence of trace amounts of $^{129}IO_3^-$. Previously made uranyl alteration phases will also be equilibrated with $^{129}IO_3^-$. The uptake of $^{129}IO_3^-$ will be studied by countermethods, x-ray diffraction, inductively coupled plasma-mass spectroscopy (ICP-MS), and inductively coupled plasma-atomic emission spectroscopy (ICP-AES). In the case of uranyl carbonates such as rutherfordine, $UO_2(CO_3)$, charge balance requirements may allow for the simultaneous incorporation of both $^{129}IO_3^-$ and $^{237}NpO_2^+$. Experiments to test for this concomitant uptake will also be performed. We anticipate that the formation of uranyl alteration phases will indeed act as a mechanism for the retardation of the release of ^{129}I. The data that we generate will be used to modify current models for the release of ^{129}I into the environment from SNF.

Approach

Most of the exploratory syntheses in recent uranyl chemistry have either been performed under ambient conditions or under hydrothermal conditions near 200°C. Conditions relevant to the Yucca Mountain repository are expected to be near 70–90°C. We will approach the incorporation of ^{237}Np and ^{129}I in two different ways. First, experiments will be performed whereby uranyl silicates, phosphates, and carbonates are crystallized in the presence of 2^{237}Np and ^{129}I. Second, we will allow previously crystallized uranyl alteration phases to equilibrate with solutions containing trace amounts of NpO_2^+ and IO_3^{1-}. Bulk product composition will be determined using powder x-ray diffraction. The uptake of radionuclides will be measured using a scintillation counter, ICP-MS, and ICP-AES. It will be important to determine the structures of actinyl iodates that crystallize at near neutral pH to show whether or not the structures of these compounds can lend some guidance in terms of which uranyl alteration products are likely to uptake IO_3^{1-}. Finally, while the solution complexation of uranyl by iodate has been studied at 25°C at low pH, data for complexation at elevated temperatures and at pH conditions similar to those expected at Yucca Mountain have not been performed. We will determine the complexation thermodynamic parameters of UO_2^{2+} with iodate at 90°C. The complexation of NpO_2^+ by iodate in solution has not been addressed at all and will also need to be done.

Accomplishments

The reactions of $^{237}NpO_2$ with excess iodate under acidic hydrothermal conditions result in the isolation of the Np(IV), Np(V), and Np(VI) iodates, $Np(IO_3)_4$, $Np(IO_3)_4{\cdot}nH_2O{\cdot}nHIO_3$, $NpO_2(IO_3)$, $NpO_2(IO_3)_2(H_2O)$, and $NpO_2(IO_3)_2{\cdot}H_2O$, depending on both the pH and the amount of water present in the reactions. Reactions with less water and lower pH favor reduced products. While the initial redox processes involved in the reactions between $^{237}NpO_2$ or $^{242}PuO_2$ and iodate are similar, the low solubility of $Pu(IO_3)_4$ dominates product formation in Pu iodate reactions to a much greater extent than $Np(IO_3)_4$ does in the Np iodate system. UO_2 reacts with iodate under these conditions to yield U(VI) iodates solely. The isotypic structures of the An(IV) iodates, $An(IO_3)_4$ (An = Np, Pu) consist of one-dimensional chains of dodecahedral An(IV) cations bridged by iodate anions. The structure of $Np(IO_3)_4{\cdot}nH_2O{\cdot}nHIO_3$ is constructed from NpO_9 tricapped trigonal prisms that are bridged by iodate into a polar three-dimensional framework structure. In uranyl iodate chemistry, we demonstrated the direct intercalation of iodic acid into the layered structure of $UO_2(IO_3)_2(H_2O)$. When $UO_2(NO_3)_2{\cdot}6H_2O$ is reacted with a two- to five-fold excess of iodic acid under mild hydrothermal conditions, the only compound that results is $UO_2(IO_3)_2(H_2O)$. When the amount of iodic acid is increased to tenfold, a mixture of $UO_2(IO_3)_2(H_2O)$ and $UO_2(IO_3)_2(H_2O){\cdot}2HIO_3$ is found.

We have also prepared several new phosphate phases, such as $Na(UO_2)(PO_4){\cdot}H_2O$, $K(UO_2)(PO_4){\cdot}2H_2O$, and

$Cs_2(UO_2)_2(PO_4)_2{\cdot}3H_2O$, that have the desired structural motifs that we need for studying the uptake of iodate. These compounds have been characterized by single crystal x-ray diffraction and other spectroscopic techniques. These compounds are similar in structure with sklodowskite, $Mg[(UO_2)(SiO_3OH)]_2(H_2O)_6$, and phurcalite $Ca_2[(UO_2)_3(PO_4)_2O_2](H_2O)_7$.

Our findings on the unusual redox chemistry of Np and Pu iodates under water-limiting hydrothermal conditions points to the importance of understanding actinide chemistry when trace amounts of water are present, as opposed to reactions when water is present in bulk amounts. The pH dependence of these reactions is also of importance in determining which oxidation state of the actinide will dominate product formation. Trace water represents a more realistic early scenario in the lifetime of a repository.

Our findings on the preparation of new phosphate phases will allow us to pursue iodate uptake studies in the final year of this grant. These studies are under way.

References

Bray, T.H., J. Ling, E.-S. Choi, J.S. Brooks, J.V. Beitz, R.E. Sykora, R.G. Haire, D.M. Stanbury, and T.E. Albrecht-Schmitt, Critical role of water content in the formation and reactivity of uranium, neptunium, and plutonium iodates under hydrothermal conditions: Implications for the oxidative dissolution of spent nuclear fuel. Inorganic Chemistry, 46, 3663–3668, 2007.

Ling, J., and T.E. Albrecht-Schmitt, Intercalation of iodic acid into the layered uranyl iodate, UO2(IO3)2(H2O). Inorganic Chemistry, 46, 346–347, 2007.

Bray, T. H.; J.V. Beitz, A.C. Bean, Y. Yu, and T.E. Albrecht-Schmitt, Structural polarity induced by cooperative hydrogen bonding and lone-pair alignment in the molecular uranyl iodate, Na2[UO2(IO3)4(H2O)]. Inorganic Chemistry, 45, 8251–8257, 2006.

Impact of Uranyl Alteration Phases of Spent Fuel on Mobility of Neptunium (Np) and Plutonium (Pu) in Yucca Mountain

Peter C. Burns
University of Notre Dame

Research Objectives

Uranyl alteration phases of spent nuclear fuel (SNF) that form in a repository such as Yucca Mountain will likely incorporate a variety of radionuclides, and will thus impact their mobility. An understanding of radionuclide incorporation mechanisms into relevant uranyl phases, as well as the structures, chemistry, and thermochemical properties of the key uranyl phases, is needed to better understand the repository source term. Ongoing research at the University of Notre Dame is mostly focused on factors that impact incorporation of ^{237}Np into selected uranyl phases that are likely to form as alteration products of SNF under moist oxidizing conditions.

Approach and Accomplishments

Synthesis and Structure of Np_2O_5

The phase Np_2O_5 has been identified as a potential solubility-limiting phase for Np^{5+} in a geological repository under oxidizing conditions. Despite its importance and simple chemistry, its structure has remained unknown. Within the framework of a detailed study of Np crystal chemistry, we developed a new synthesis technique that provides single crystals of Np_2O_5 via a mild hydrothermal route and determined its structure using single-crystal X-ray diffraction. The details of this study have been published in Forbes et al. (JACS 129, 2760–2761). The structure, shown in Figure 1, contains neptunyl square and pentagonal bipyramids that are linked into a layered framework. The formation of this compound under such mild conditions should have a significant impact on modeling the fate and transport of this radionuclide in the environment. These results for Np_2O_5 will also allow further characterization in terms of thermodynamic stability and ultimately a reassessment of its role in the environmental chemistry of Np.

Incorporation of Np^{5+} Into Single Crystals of Uranyl Phases

Our earlier studies have examined incorporation of Np^{5+} into synthetic powders of uranyl phases. The results of these studies indicate that Np is incorporated into some structures, whereas others (those containing electroneutral sheets and no interlayer cations) largely exclude Np.

We have synthesized single crystals of 10 uranyl phases using solutions containing 500 ppm Np^{5+}. These phases were selected to provide a substantial range of crystal structure connectivities, as well as multiple sites for potential incorporation of Np^{5+}. Recovered crystals were analyzed initially by single crystal x-ray diffraction to verify their identities. Subsequently, each was analyzed using laser-ablation inductively coupled plasma mass spectrometry (LA-ICP-MS), which was used to measure the ratio of mass 237 (Np) to 235 (U) (U-235 is present at about 0.2%). Analyses of crystals that were synthesized in the absence of Np consistently gave a background ratio of 0.0004. Analyses of the ten compounds all revealed substantial incorporated Np. These results show unequivocally that the Np is located within the crystals of the uranyl phases. The level of incorporation

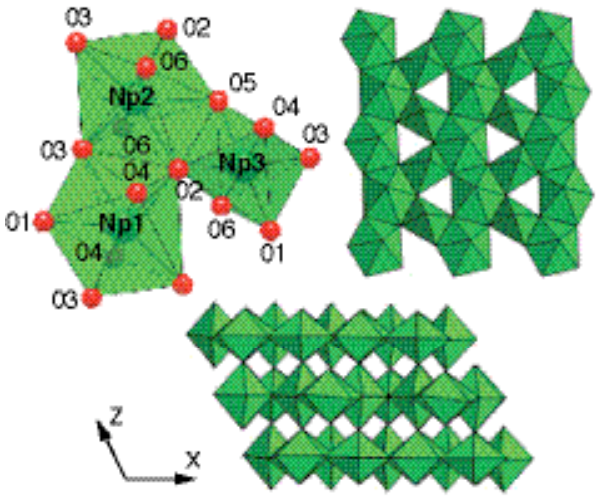

Figure 1. Polyhedral representation of the crystal structure of Np_2O_5

was found to vary considerably over the compounds studied, and there was no apparent correlation with the synthesis conditions utilized in each case. Rather, the connectivity of the crystal structure and the availability of different types of cation sites appear to be the factors that impact incorporation. Ongoing studies of additional phases are currently under way to further elucidate the

structural controls on Np^{5+} incorporation. A representative crystal and ICP-MS data are given in Figure 2.

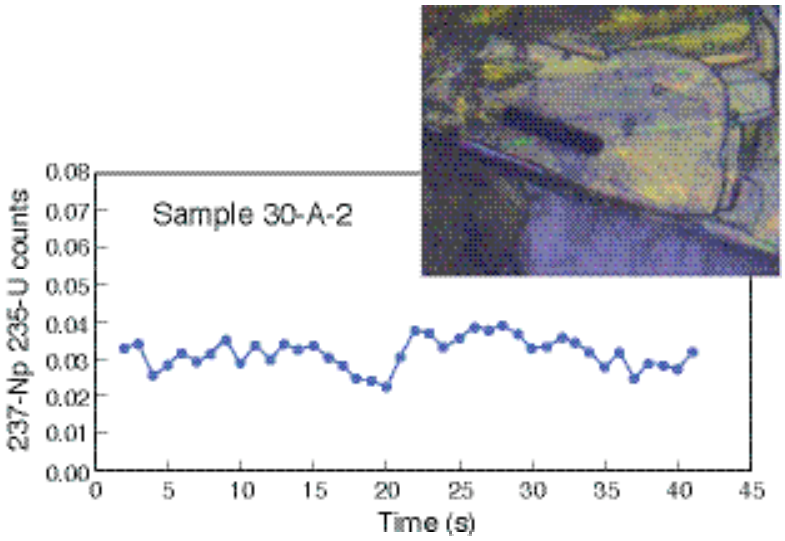

Figure 2. Representative example of a single crystal of a uranyl phase synthesized in the presence of Np^{5+}, and the corresponding LA-ICP-MS data showing the ratio of counts for mass 237 (Np) and 235 (U).

Crystal Chemistry of Perrhenate as an Analogue for Pertechnetate

It has often been assumed that pertechnetate will not complex uranyl ions in solution, and that pertechnetate cannot coordinate uranyl ions in crystal structures, owing to the bond-valence requirements of the pertechnetate group (e.g., Chen, Burns, and Ewing, J. Nucl. Mater. 2000, v.278, 290–300). It is therefore assumed that pertechnetate will not be incorporated into uranyl phases that form when SNF is altered in a geological repository. However, over the past three years, several studies have appeared in the literature that unequivocally show that perchlorate, perrhenate, and pertechnetate can all coordinate uranyl ions. These studies have been a combination of spectroscopic and diffraction analysis, and have focused on compounds containing uranyl ions and a range of organic molecules.

We developed techniques for the synthesis of single crystals of uranyl perrhenates, as crystal-chemical analogues for uranyl pertechnetates. Thus far, these techniques have yielded the crystal structures of the compounds $(UO_2)_2(ReO_4)_4(H_2O)_3$, $[(UO_2)_4(ReO_4)_2O(OH)_4(H_2O)7](H_2O)_5$, and $Na(UO_2)(ReO_4)_3(H_2O)_2$. Each of these compounds contain uranyl ions that are coordinated by perrhenate groups. The first contains chains of uranyl pentagonal bipyramids that are bridged by the sharing of equatorial vertices with perrhenate groups, whereas the latter two contain isolated clusters of uranyl pentagonal bipyramids that share vertices with perrhenate groups. These structures firmly establish the possibility of coordination of uranyl by perrhenate, and strongly suggest that pertechnetate can also coordinate uranyl. This suggests that pertechnetate may be incorporated into some uranyl minerals by substitution for tetrahedrally coordinated cations, and experimental studies of such incorporation are warranted.

Actinide Adsorption to U(VI) Silicates

S. B. Clark[1] and Lawrence C. Hull[2]
[1]Washington State University | [2]Idaho National Laboratory

Research Objectives

Recent work by us and others indicates that actinide adsorption to the U(VI) solids expected in the waste package may play a key role in the reduction of dissolved concentrations of radionuclides such as Np(V). However, little is known about the mechanism(s) of adsorption, nor is there sufficient knowledge or data to represent the phenomenon in predictive modeling codes. Unfortunately, this situation makes it impossible to consider actinide adsorption to the U(VI) silicates in either geochemical or performance assessment (PA) predictions.

The goal of this project, initiated on August 15, 2005, is to develop a thermodynamic description of the adsorption of key actinide cations to relevant U(VI) silicates using a surface complexation approach. Our objectives are to:

1. *Study the surface charge associated with well-characterized U(VI) silicate solids* under chemical conditions representing the waste package after corrosion.
2. *Develop thermodynamic data to describe the adsorption of actinide cations to well-characterized U(VI) silicate solids.* Adsorption and desorption experiments are conducted under conditions designed to address the complexity of the waste package chemistry.
3. *Verify surface charge behavior and adsorption processes/mechanisms with appropriate spectroscopic tools.* We are developing a molecular description of surface roughness and actinide sequestration at U(VI) silicate surfaces.
4. *Use experimental results to parameterize a geochemical model to describe actinide sorption to U(VI) silicate solids.* This surface complexation approach will use the diffuse double layer model that can be incorporated into geochemical codes such as EQ3/6.

Approach

Our overall approach is to assume that the interaction of the positively charged actinide cations to the surface of U(VI) silicates is driven by electrostatics. Thus, one of the most important parameters for understanding the sorption of contaminants to surfaces is the electrostatic charge of that surface as a function of pH and ionic strength. Our conceptual model for the U(VI) silicate surfaces available as complexation sites for the actinide cations is shown in Figure 1. Similar to the approach used routinely for clay minerals, we are considering both surface sites and edge sites. These are the sites that can be protonated or deprotonated, thereby leading to surface charge, and also sites that can complex actinide cations.

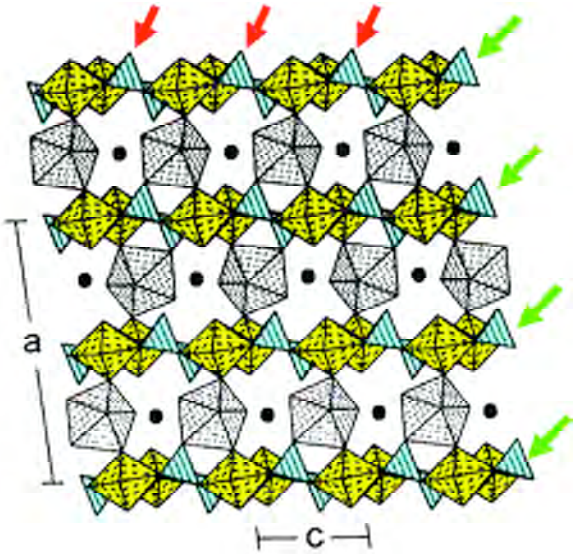

Figure 1. Possible sites for surface complexation of NpO_2^+ or other actinide cations to the α-uranophane structure. The green arrows show locations at the edge of each sheet; the blue tetrahedral are the silicate moieties, which can complex actinide cations. The red arrows show another possibility for coordination to the silicate tetrahedra located within the sheet.

Accomplishments

We have begun to measure the surface charge of the U(VI) silicate series uranophane ($Ca[(UO_2)(SiO_3OH)]_2\ (H_2O)_5$), Na-boltwoodite ($Na[(UO_2)(SiO_3OH)](H_2O)S$), and sklodowskite ($Mg[(UO_2)(SiO_3OH)]_2(H_2O)_6$). Our preliminary results are shown in Figure 2. In the pH region of 5–7, the surface charge changes significantly, as expected. Interestingly, our initial results suggest that these surfaces are negatively charged at all pH values, although at pHs

below 5, the charge is only slightly negative. Above pH 7, the surface has a relatively high negative charge. In the region between pH 5–7, the surface charge varies markedly. Also, although all the U(VI) silicate surfaces show very similar behavior, note that the sklowdowskite surface is less negatively charged at a given pH than uranophane or boltwoodite.

Based on these results, we have begun experiments to determine Np(V) adsorption isotherms to these U(VI) solids. We expect that adsorption at pH values less than 5 will be quite low, that it will increase above pH 5, and that it should reach 100% by pH 7. As the simple dissolved cation, NpO_2^+ has a low cationic charge, which we suspect will limit its overall ability to sorb to the surface. We will consider changes in the Np(V) speciation as a function of pH over that region.

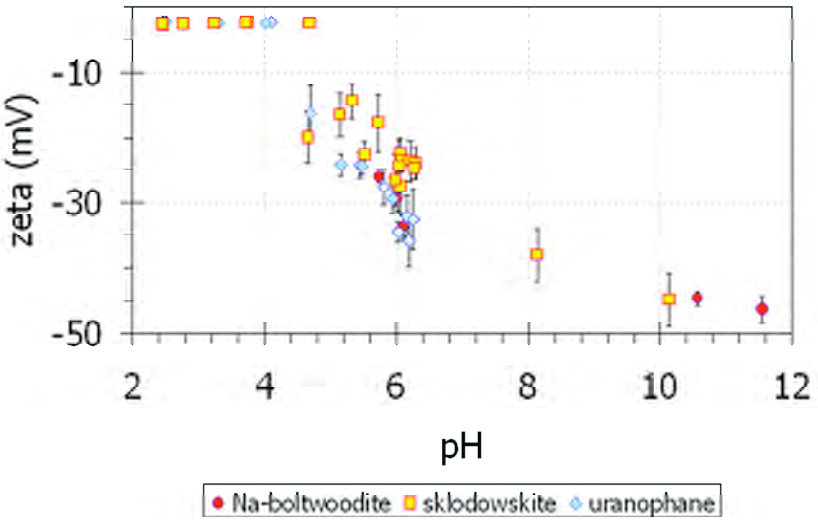

Figure 2. The measured zeta potential for Na-boltwoodite, sklodowskite, and uranophane as a function of pH. Note that in all cases, the zeta potential is negative. In the pH region of 5–7, sklodowskite is less negative at a given pH value than Na-boltwoodite or uranophane.

The sorption isotherms will be treated with a two-site model, as described above. We intend to use x-ray absorption spectroscopy to verify our assumptions about the molecular level interaction of the actinide cation to the U(VI) silicate surface.

Adsorption of Np and other actinides to U(VI) solids likely reduces their dissolved concentrations significantly. Unfortunately, little is known about actinide adsorption to these solids, and consequently, this phenomenon is not currently considered in the Yucca Mountain performance assessment. Our initial results suggest that while all of these solids have a capacity to sorb actinide cations at all pH ranges, sklowdowskite at near neutral pH values is less negatively charged than the other U(VI) silicates. This indicates that in this pH region, boltwoodite and uranophane may be more important solids than sklodowskite for sorption of the actinides. The knowledge and data gained by this science project will address this opportunity to improve the Yucca Mountain performance assessment.

Corrosion of Spent Nuclear Fuel: The Long-Term Assessment

Rodney C. Ewing
University of Michigan

Research Objectives

Spent nuclear fuel (SNF), essentially UO_2, accounts for over 95% of the total radioactivity of all of the radioactive wastes in the United States that require disposal, disposition, or remediation. The alteration of SNF results in the formation of new uranium phases that can cause the release or retardation of actinide and fission-product radionuclides. Over the long term, and depending on the extent to which the secondary uranium phases incorporate fission products and actinides, *these alteration phases become the near-field source term.*

This research program is a broadly based effort to understand the long-term behavior of SNF and its alteration products in a geologic repository. This research program addresses the following questions: (1) What are the *long-term* corrosion products of natural UO_{2+x}, uraninite, under oxidizing and locally reducing conditions? (2) What is the sequence of formation of the phases during alteration? (3) What is the radionuclide content of the corrosion products, as compared with the original UO_{2+x}? and (4) What are the effects of ionizing radiation and alpha-decay on the stability and composition of the U(VI)-phases?

Approach

The research program at the University of Michigan was initiated in July of 2004. At present we have one graduate student, Elizabeth Anderson (OCRWM Fellowship; NSF Fellowship) and three post-doctoral fellows, Satoshi Utsunomiya, Artur Deditius, and Veronique Pointeau (CEA). We have initiated studies in three areas: (1) studies of the alteration phases of UO_2 under oxidizing and reducing conditions; (2) evaluation of the role of colloids in radionuclide transport; (3) heavy-particle and ionizing radiation damage of U(VI)-phases; (4) experiments that use mockups to study the interactions of radionuclides with the corrosion products of the waste packages (in collaboration with Sandia National Laboratory).

Accomplishments

Alteration of Coffinite ($USiO_4$) Under Reducing and Oxidizing Conditions

Coffinite ($USiO_4 \cdot nH_2O$, $I4_1/amd$, Z=4) is a major alteration phase of uraninite, UO_{2+x}, under reducing conditions. This work is focused on (1) characterization of the alteration of coffinite under reducing and oxidizing conditions, and (2) determination of the role of organic matter during precipitation and alteration of coffinite. We have examined natural, coarse-grained coffinite from the Grants uranium region, New Mexico. The coffinite samples have been analyzed in detail at the submicron scale, in order to understand the microscale evolution of texture and chemistry during alteration under reducing and oxidizing conditions.

Two different populations of coffinite were identified. The primary coffinite grows on the mixed layers of organic matter and V-mica, mainly roscoelite $[K(V,Al,Mg)_2AlSi_3O_{10}(OH)_2]$, while secondary coffinite is present on the surfaces of the primary coffinite. Based on the electron-microprobe analyses (EMPA), chemical formulas of primary and secondary coffinites are:

$$(U_{0.924}Ca_{0.218}REE_{0.026})_{1.168}(Si_{0.835}P_{0.033}As_{0.010})_{0.868}O_4 \cdot nH_2O$$

$$(U_{0.805}Ca_{0.156}REE_{0.027}Zr_{0.001})_{0.988}(Si_{0.954}P_{0.036}As_{0.005})_{0.990}O_4 \cdot nH_2O$$

The concentrations of U, Ca, and As decreased, whereas Si, P, and REEs were incorporated into the structure during the recrystallization of secondary coffinite under reducing conditions. Analysis totals by EMPA for both primary and secondary coffinite are variable and high (93.7–99.1 wt% and 91.9–99.7 wt%, respectively), indicating that H_2O is not an essential component of the coffinite structure. Under oxidizing conditions, coffinite altered to form (Na,K)-boltwoodite $[(Na,K)(UO_2)(SiO_3OH)(H_2O)_{1.5}]$ and subsequently to uranyl sulfates. In a few cases, coffinite was directly altered to U-sulfate, which is tentatively identified as jáchymovite $[(UO_2)(SO_4)(OH)_{14}(H_2O)_{13}]$.

Based on charge-balance calculations using EMPA data, the coffinite can incorporate small amounts of U^{6+} up to 0.2 [apfu]: $(U^{4+}_{1-x}U^{6+}_x)Si_{1-x}O_4 \cdot nH_2O$, $0<x<0.2$. In order to balance the charge, $(OH)^-$, groups can be introduced into the Si position. These substitution mechanisms are expressed as:

$$U^{4+} + Si^{4+} \leftrightarrow U^{6+} + 2(OH)^-$$
$$(Y,REE)^{3+} + (P,As)^{5+} \leftrightarrow U^{4+} + Si^{4+}$$

Colloid Transport of Actinides

Sorption of actinides, particularly plutonium, onto submicron-sized colloids increases their mobility in the environment. Because of their low concentrations (<ppm), their occurrence and speciation on colloids in the "far field" have not yet been described. Based on the systematic analyses of the solid and the solution, we have investigated actinides on colloids in the groundwater from the Mayak Production Association, Urals, Russia, where at "ground zero" the Pu-activity is ~1000 Bq/l. Pu-activities are still 0.16 Bq/l (3 km) with 70–90 mol% of the Pu sorbed onto nanocolloids, confirming the significant role of colloids in the transport of Pu over long distances. Nano-SIMS elemental maps reveal that amorphous Fe-oxide colloids adsorb Pu(IV)-hydroxides or -carbonates along with U-carbonates.

Radiation Effects on U^{6+} Phases

U(VI) phases are common alteration products of SNF under oxidizing conditions, and they may potentially incorporate actinides, such as long-lived ^{239}Pu and ^{237}Np, delaying their transport to the biosphere. In order to evaluate the effects of ballistic interactions of α-decay events and ionizing radiation by β-decay on the stability of the U^{6+}-phases, we have conducted ion-beam (1.0 MeV Kr^{2+}) and electron-beam irradiations on six different structures of U(VI) phases: uranophane, kasolite, boltwoodite, saleeite, carnotite, and liebigite, in addition to uranyl oxide hydrate, schoepite. Under ion-beam irradiation, nanocrystals of UO_2 formed at doses as low as 0.006 dpa, which is slightly less than the accumulated dose in pure U^{6+} phases due to self -decay after 100,000 years, 0.009 dpa, and much less than the estimated dose after 10,000 years for the case that 1 wt.% ^{239}Pu is incorporated. During electron irradiation of schoepite, the amorphization dose (D_c) was only 0.51×10^{10} Gy, and randomly oriented uraninite nanocrystallites formed at 7.8×10^{10} Gy, which is approximately the same dose as compared with the D_cs for the other U^{6+}-phases. Because the predicted cumulative dose from ionizing radiation in SNF is ~10^7–10^8 Gy during the first $10^{2–3}$ years after discharge, U^{6+}-phases are not expected to amorphize during this time.

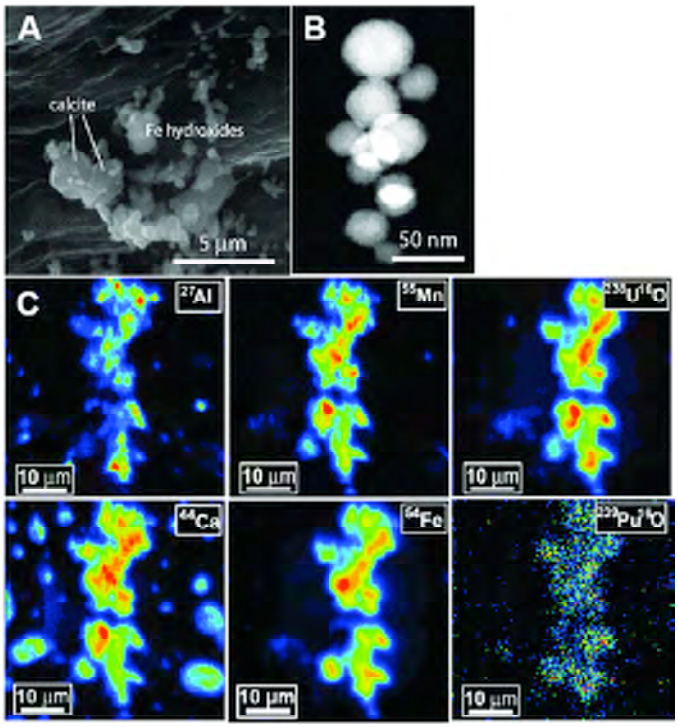

Figure 1. Direct evidence of Pu-adsorption onto amorphous Fe-hydroxyoxide. (A), SEM micrograph of typical colloids from well #1/69. Many spherical particles were observed with a size of < 1 µm. (B), high-angle annular dark-field scanning TEM image of the spherical colloids. Electron diffraction patterns from these particles indicate that they are amorphous. (C), Contrast-enhanced, nano-SIMS elemental maps. (The intensity of the color does not correspond to the concentrations of the different elements [after Novikov et al., 2006].)

References

Novikov, A.P., S.N. Kalmykov, S. Utsunomiya, R.C. Ewing, F. Horreard, S.B. Clar, V.V. Tkachev, and B.F. Myasoedov, Colloid transport of plutonium in the far-field of the Mayak Production Association, Russia. Science, 314, 638–641, 2006.

Utsunomiya, S., and R.C. Ewing, Radiation-induced decomposition of U(VI) alteration phases of UO_2. Proceedings of the Material Research Society Symposium, 932, 465–472, 2006.

Figure 2. Selected area electron diffraction patters showing the transition in schoepite as a function of the cumulative ionizing dose. After Utsunomiya and Ewing (2006).

Direct Determination of the Thermodynamic Properties of Uranyl Minerals Important for the Performance of the Proposed Geological Repository at Yucca Mountain

Jeremy B. Fein[1], Peter C. Burns[1], and Alexandra Navrotsky[2]
[1]University of Notre Dame | [2]University of California, Davis

Research Objectives

The objective of this study is to determine the thermodynamic properties for a broad range of environmentally important uranyl mineral phases using solubility and calorimetric measurements, producing an internally consistent dataset that is useful in modeling spent nuclear fuel (SNF) alteration and U mobility behavior in near-surface environments.

We are using solubility and calorimetry measurements in order to provide rigorous constraints on the Gibbs free energies of formation, enthalpies of formation, and standard entropies for these solids. These parameters are needed not only to determine which uranyl phases will become stable as a function of conditions as SNF alters in a repository setting, but also to calculate the mobility of U in equilibrium with these alteration phases. Solubilities of representative members of the uranyl oxide hydrates, uranyl silicates, and uranyl carbonates are being measured both for the end-member phases as well as for selected phases containing a range of substituted Np within the crystal structure.

Approach

In the experimental research program, we are synthesizing and measuring the solubility of a wide range of uranyl mineral phases. In order to improve the accuracy and precision of the thermodynamic interpretation of the data, solubility measurements are being conducted primarily under the low pH conditions at which UO_2^{+2} is the dominant aqueous uranyl species. The solubility experiments are being conducted as functions of pH, ionic strength, and temperature, and will yield Gibbs free energies of formation of the phases of interest. The calorimetric data will enable determination of the enthalpies of formation for these phases, so together the standard entropies can be determined as well.

The mineral syntheses and solubility measurements are being conducted at University of Notre Dame under the supervision of Burns and Fein, respectively; the calorimetry measurements are being conducted at University of California-Davis under the supervision of Navrotsky.

Solubility Experiments

Successful extraction of thermodynamic data from solubility measurements requires a range of measurements or controls on the experimental systems: (1) rigorous demonstration of equilibrium reversal; (2) measurements of the equilibrium pH and the total equilibrium concentrations of all mineral-forming cations in the system; (3) ionic strength control or measurement; and (4) determination that secondary mineral phases do not form during experimentation. In each batch solubility experiment, a synthesized uranyl mineral powder is placed in contact with a fixed ionic strength solution, and the pH of the suspension is adjusted to a desired value using minute volumes of concentrated perchloric acid or sodium hydroxide solution. Samples are taken as a function of time and analyzed for dissolved cations using an inductively coupled plasma optical emission spectroscopy approach. The solids used in each experiment are analyzed using x-ray diffraction and Fourier-transform infrared spectroscopy to check for secondary precipitates that may have formed during the experiments. In some experiments, solubility reversals are conducted by spiking the starting solutions with uranium and any other mineral-forming cations, so that equilibrium is approached from supersaturation.

Calorimetry Experiments

High-temperature oxide melt solution calorimetry uses a Calvet-type high temperature custom-built calorimeter. Solution enthalpies for each sample are measured by dropping ~5 mg pressed pellets of material from room temperature, 298 K, into the molten oxide solvent, $3Na_2O\text{-}4MoO_3$, at calorimetric temperature, 976 K. The calorimeter, calibrated using the heat content of $\alpha\text{-}Al_2O_3$, is flushed continuously with O_2 throughout the experiments to ensure an oxidizing atmosphere. Prior to the calorimetric experiments, complete dissolution in the solvent at calorimetric conditions is established in a furnace at 976 K. A large and rapidly generated endothermic enthalpy of drop solution for each phase, return of the calorimetric signal to its baseline value, and a solvent color change from white to yellow indicates that the uranyl minerals dissolve fully in the melt. The high density of the sample assures that the pellets drop quickly and sink in the solvent, so that the sam-

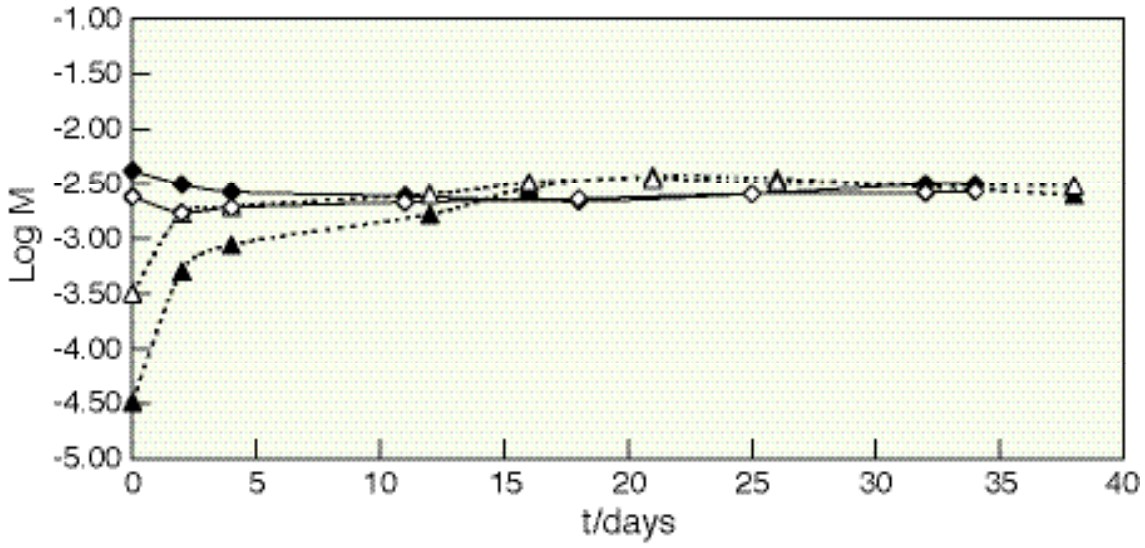

Figure 1. . Plot of logarithm of solubility of soddyite against time for experiments at pH 3.67 from supersaturation (filled diamonds U and open diamonds Si) and undersaturation (filled triangles U and open triangles Si). These results, in conjunction with calorimetry measurements, place tight constraints on the thermodynamic properties that define soddyite stability and solubility under a range of repository conditions.

ple does not float on the surface of the melt. Calorimetry is straightforward and problem-free. We are conducting calorimetry measurements on each of the phases used for solubility experiments that have not previously been examined using calorimetry.

Accomplishments

Over the past year, we have perfected synthesis techniques for a number of uranyl oxide hydrates, uranyl silicates, and uranyl carbonates, and solubility and calorimetry measurements have been conducted on several of these phases. Solubility measurements indicate that solubility reversals can be measured and equilibrium attained over the course of 10–20 days, depending on pH and the uranyl phase present. We have also begun synthesis and solubility experiments to study the effect of Np-incorporation in soddyite on the concentrations of U and Np in equilibrium with the mixed neptunyl/uranyl phase. Our solubility and calorimetry measurements for pure soddyite are reported in the first publication from this project in *Journal of Chemical Thermodynamics* (Figure 1). Five additional papers are in preparation: one which will review what is known about solubilities and thermodynamic properties of uranyl minerals; one experimental paper on each of the following groups of minerals—the uranyl silicates, the uranyl hydrates, and the uranyl carbonates—and a publication on the solubility of soddyite with incorporated Np. All papers should be completed and submitted this year.

The results from this project will dramatically improve our understanding of the thermochemical parameters of uranyl minerals, thereby improving our ability to model radionuclide mobility in the subsurface. The experiments in this study are valuable as direct indications of the concentration of uranium and other elements in solution in equilibrium with environmentally important uranyl mineral phases. In addition and perhaps more importantly, the experiments yield an internally consistent dataset of the thermodynamic properties for a wide range of uranyl minerals of repository and general environmental interest.

Project Publication

Gorman-Lewis, D., L. Mazeina, J.B. Fein, J.E.S. Szymanowski, P.C. Burns, and A. Navrotsky, Thermodynamic properties of soddyite from solubility and calorimetry measurements. Journal of Chemical Thermodynamics, 39, 568–575, 2007.

Chemical and Coordination Structure of Radionuclides in Spent Nuclear Fuel and Its Alteration Products: Understanding Release Pathways

Jeffrey A. Fortner, A. Jeremy Kropf, and James C. Cunnane
Argonne National Laboratory (ANL)

Research Objectives

Knowledge of the chemical states of trace fission products and transuranium actinides in spent nuclear fuel (SNF) and related materials from the nuclear fuel cycle provide insight that may benefit both modeling and design considerations for waste disposal in a geologic repository. Owing to the overall complexity of the repository system, it is important to establish multiple lines of evidence for a proposed mechanism to describe radionuclide behavior. To this end, this project examining SNF materials was designed to complement independent thermodynamic and solution chemistry experiments. Of the available techniques, x-ray absorption spectroscopy (XAS) was found to be uniquely suited for determining oxidation states and structural environments of elements in solids, particularly within challenging radioactive specimens. This project was initiated to investigate the solid state chemistry of radioactive fission products (e.g., technetium) and activation products (neptunium, plutonium) in SNF by using advanced XAS techniques, many of which were developed as part of this project. The objective is to provide definitive information about the crystal chemistry of these key radionuclides and to determine the possible impact on release behavior during SNF corrosion. We also address possible sequestration of these radionuclides in more stable minority phases (e.g., exsolved, metallic 5-metal "epsilon" particles) and secondary alteration phases. Technetium-99 (^{99}Tc) is an important radionuclide in repository models, owing to its relatively long half-life and the high aqueous solubility of its compounds where it is in the heptavalent state. As oxide SNF undergoes fission in a reactor, a portion of the technetium is incorporated into an exsolved intermetallic "epsilon particle" alloy that forms in the fuel from the 5th-period noble metal fission products molybdenum, technetium, ruthenium, rhodium, and palladium.

By strengthening the science underlying models developed to predict the long-term performance of SNF in the planned repository, we hope to provide insight that is expected to benefit both modeling and design considerations for waste disposal in a geologic repository.

Approach

In order to obtain spectroscopic information from elements present in SNF at the trace level and in the presence of an intense x-ray fluorescence background from the uranium oxide matrix, an energy discriminating detector based upon diffractive optics, the "bent-Laue analyzer" (BLA) detector, was chosen. At the time this project was initiated, the BLA concept had been demonstrated, but needed further improvements to be developed under the auspices of this project. Among the improvements developed were refined optics to achieve microprobe x-ray spot size to smaller than 2 microns at 19 keV, using new mirrors that were specifically designed to be used with the BLA, and a quad-analyzer array to obtain simultaneous, independent tuning and data acquisition. Using this approach, detailed XAS information from technetium and other trace elements in specimens of SNF has been obtained. By analyzing XAS extended fine structure (EXAFS) data from a particular absorption edge, we can determine the local environment of a specific atomic species, including distances to near-neighbors, types and numbers of neighboring atoms, and details of the radial distribution function. The energy of the absorption threshold and near-edge absorption features also can be used to obtain information about the charge state of the central atom and the site symmetry.

Accomplishments

Several XAS measurements from SNF and separate epsilon-phase alloys were performed at the Materials Research Collaborative Access Team (MR-CAT) insertion device beamline, located at the Advanced Photon Source (APS), a third-generation x-ray synchrotron source at Argonne National Laboratory. The brightness of the APS in the high-energy x-ray regimes makes it ideal for investigating these materials, which have relatively high-energy absorption edges for key elemental components, and which must be carefully encapsulated for radiological safety. Specimens were obtained from SNF used in testing for the Yucca Mountain Project; from SNF-derived epsilon metal particles that had been chemically separated from fuel by Daqing Cui of Studsvik Nuclear AB, Sweden, with whom we have an ongoing collaboration (Figure 1); and from synthetic epsilon metal prepared by arc-melting Mo, Ru, Rh, and Pd (with Re as a stand-in for Tc) provided by David Wronkiewicz of the University of Missouri-Rolla (Figure 2). Among the observations is that the epsilon phase in SNF has been found to persist relatively intact in corroded SNF,

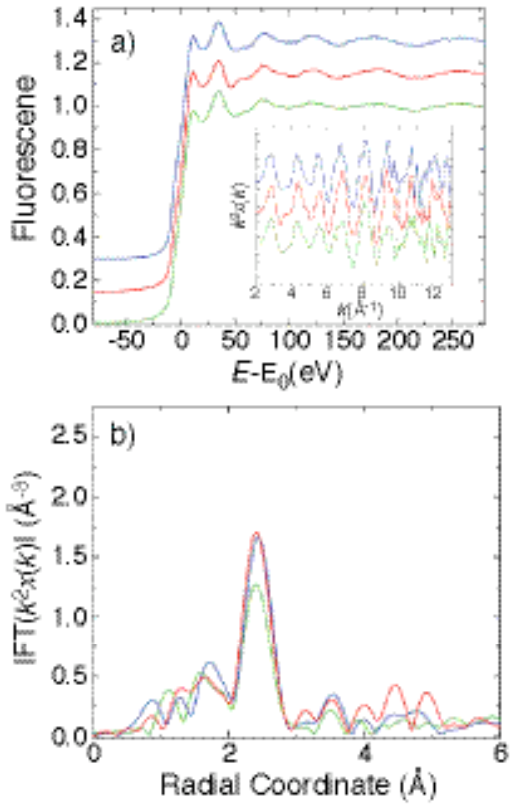

Figure 1. EXAFS from epsilon metal particles extracted from spent fuel by Daqing Cui et al. a) Spectral edges from Mo (blue) Tc (red) and Ru (green) with fine structure (inset). b) Fourier transform modulus with color key as in a). Note the striking similarity of the near-edge and fine structure, suggesting a very well-mixed alloy.

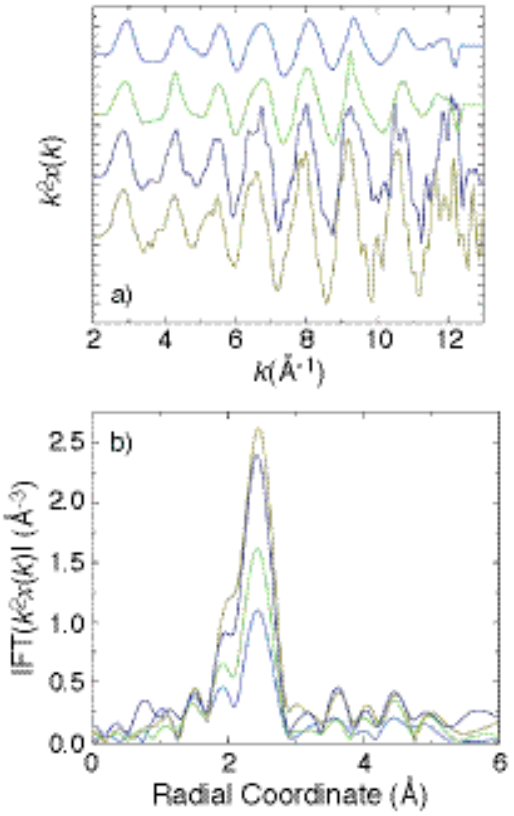

Figure 2. a) X-ray absorption fine structure from Mo, Ru, Rh, and Pd (in order from top to bottom) in a synthetic epsilon particle *sans* Tc from the University of Missouri-Rolla (courtesy D. Wronkiewicz). b) Fourier transform moduli, with peak amplitude in order of decreasing intensity representing Pd (olive) Rh (navy) Ru (green) and Mo (blue). In this specimen, the Mo appears substantially less well-ordered than the more noble metals, and less ordered than the Mo in the CSNF-derived epsilon phase (Figure 1).

with little evidence of de-alloying (loss of less-noble metals molybdenum and technetium). This suggests that the corrosion potential of the bulk fuel is fixed below the de-alloying potential of the epsilon metal. Also, the epsilon phase may be difficult to simulate in detail outside of the irradiated fuel (Figure 2). This may be owing to the conditions of high irradiation and prolonged time at temperature under which the epsilon phase forms in the fuel.

References

Cui, D., J. Low, C.J. Sjöstedt, and K. Spahiu, On Mo-Ru-Tc-Pd-Rh-Te alloy particles extracted from spent fuel and their leaching behavior under Ar and H2 atmospheres. Radiochim. Acta, 92, 551–555, 2004.

Fortner, J.A., A.J. Kropf, J.L. Jerden, and J.C. Cunnane, Chemical effects at the reaction front in corroding spent nuclear fuel. In: Scientific Basis for Nuclear Waste Management XXX, D.S. Dunn, C. Poinssot, and B. Begg, eds., Mater. Res. Soc. Symp. Proc. 985 Paper 0985-NN01-03, Warrendale, PA, 2007.

Fortner, J.A., A.J. Kropf, R.J. Finch, and J.C. Cunnane, Technetium and molybdenum in oxide spent nuclear fuel: Impact on release estimates. In: Scientific Basis for Nuclear Waste Management XXVIII, J.M. Hanchar, S. Stroes-Gascoyne, and L. Browning, eds., Mater. Res. Soc. Symp. Proc. 824, Paper CC2.11 Warrendale, PA, 2004.

Fortner, J.A., R.J. Finch, A.J. Kropf, and J.C. Cunnane, Re-evaluating neptunium in uranyl alteration phases from corroded spent fuel. Nuclear Technology, 148 (2), 174–180, 2004.

Fortner, J.A., A.J. Kropf, R.J. Finch, C.J. Mertz, J.L. Jerden, M.G. Goldberg, and J.C. Cunnane, Analysis of trace elements in commercial spent nuclear fuel using X-ray absorption spectroscopy. In: *Global 2003*, ANS Proceedings, 2003.

Kropf, A.J., J.A. Fortner, R.J. Finch, J.C. Cunnane, and C. Karanfil, A bent silicon crystal in the Laue geometry to resolve X-ray fluorescence for X-ray absorption spectroscopy. Physica Scripta, T115, 998–1000, 2005.

Wronkiewicz, D.J., C.S. Watkins, A.C. Baughman, F.S. Miller, and S.F. Wolf, Corrosion testing of a simulated five-metal epsilon particle in spent nuclear fuel. In: Scientific Basis for Nuclear Waste Management XXV, B.P. McGrail and G.A. Cragnolino, eds., Mat. Res. Soc. Symp. Proc., 713, Paper JJ14.4.2., 2002.

An *In Situ* Spectroelectrochemical Study of Neptunium (Np) Redox, Dissolution, and Precipitation Behavior at the Corroding Spent Nuclear Fuel/Alteration Phase Interface

Artem Guelis[1], Jeremy Kropf[1], Christopher Johnson[1], Jeffrey Fortner[1], and Petr Vanysek[2]
[1]Argonne National Laboratory (ANL) | [2]Northern Illinois University

Research Objectives

The objective of this project is to examine the oxidative dissolution of Np(IV) and the reductive precipitation of aqueous Np(V) species at $U_{(1-x)}Np_xO_2$ [$0 \le x < 0.1$] and other surfaces under applied oxidation potential conditions relevant to the range of corrosion potentials expected for the surface of corroding spent UO_2 fuels in air-saturated solutions (i.e., at applied potentials near the fuel's corrosion potential).

In spent UO_2 fuels Np is expected to be present as a solid solution of NpO_2 in the UO_2 fluorite structure, with which it is compatible. Np may be released from the spent UO_2 fuels matrix when the matrix degrades by oxidative dissolution. Available data in acidic solutions indicate that the standard potential for the UO_2^{2+}/U^{4+} is significantly lower than the standard potential for the NpO_2^{+}/Np^{4+} couple, and indicate that reduction of Np(V) by U(IV) as the fuel corrodes is thermodynamically favored, as shown by the following reaction:

$$2NpO_2^{+} + U^{4+} + 4H^{+} = 2\,Np^{4+} + UO_2^{2+} + 2H_2O$$
$$E^o = 0.405 \text{ to } 0.469V$$

Although this equilibrium equation is not valid for the solid-liquid interface, the spent nuclear fuel (SNF) corrosion potential is expected to be lower than the potential of the Np(V)/Np(IV) couple, so one could expect the reduction of Np(V) at the SNF surface. This indicates that oxidation of Np(IV) in the fuel's lattice may not occur under the pertinent potential conditions at the fuel's surface. In short, the oxidative dissolution behavior of Np at the corroding fuel surface remains uncertain.

Approach

The work included the following objectives: (1) determine the applied potential range for reductive precipitation of Np(V) onto $U_{(1-x)}Np_xO_2$ [$0 \le x < \sim 10^{-1}$] and inert (e.g., Pt, carbon or pyrolytic graphite) electrode surfaces; (2) identify the applied potential ranges for congruent and incongruent release of Np(V) and U(VI) from $U_{(1-x)}Np_xO_2$ surfaces; and (3) design electrochemical cells suitable for performing the Np oxidative dissolution and reductive precipitation measurements *in situ* at Argonne's Advanced Photon Source (APS) Materials Research–Collaborative Access Team (MR-CAT) beamline; and (4) conduct x-ray absorption near-edge structure (XANES) and extended x-ray absorption fine structure (EXAFS) analyses of solution species and precipitated solids at $U_{(1-x)}Np_xO_2$ solid-liquid interfaces.

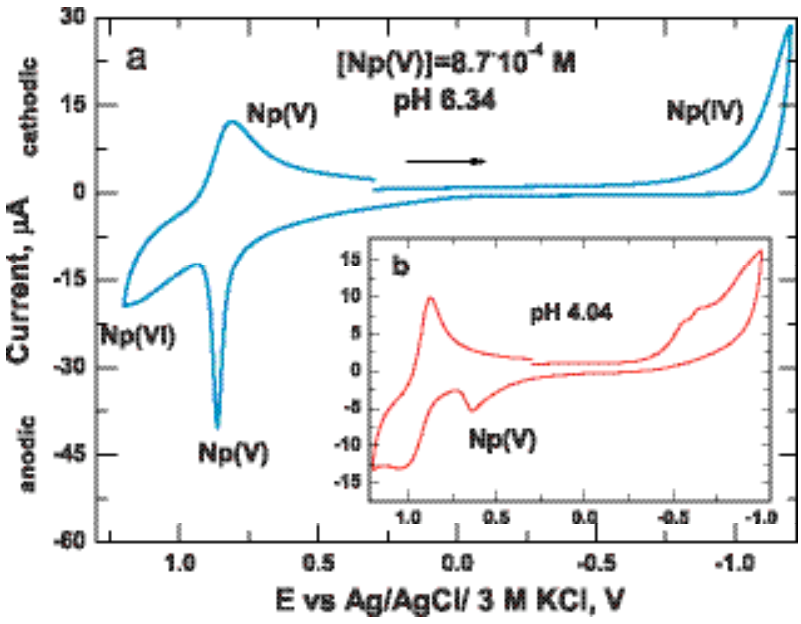

Figure 1. Cyclic voltamogram of Np in 0.1 m NaCl on glassy carbon electrode (a) pH 6.34, (b) pH 4.04.

Accomplishments

Using cyclic voltametry of the Np solution at neutral pH, we have determined the potential range for the reductive precipitation of Np(V) to Np(IV) on the glassy carbon and Pt working electrodes, with consecutive oxidation of Np(IV) oxo-hydroxy species from the electrode surface to soluble NpO_2^{+} species (Figure 1).

As expected, a significant overpotential is observed for the electron transfer between Np(V) and Np(IV), due to

the changes in the chemical structures. The Np(VI)/Np(V) couple, on the other hand, reveals reversible behavior at lower pH and quasi-reversible behavior in neutral solutions.

The reduction of Np(V) at the UO_2 surface without applied potential was demonstrated by allowing the $^{238}UO_2$ pellet to react with air-saturated neutral Np(V) solution for 4 days. XANES analysis showed the presence of a mixture of Np(IV) and Np(V) precipitated at the UO_2 surface (Figure 2). The Np concentration in the solution decreased from 1×10^{-4} to 3.3×10^{-5} M.

We have designed and built an electrochemical cell for laboratory and synchrotron use. In addition to standard fluid and electrode ports for electrochemistry, two inline x-ray windows allow beam access at glancing incidence to the electrode surface. A third larger window parallel to the electrode surface may be used as a beam port or as a fluorescence/scattering exit. *In situ* x-ray glancing incidence and reflectivity measurements, as well as x-ray absorption spectroscopy and limited x-ray diffraction measurements, are possible using this cell with this window configuration. The positioning of the electrode with respect to the larger window was expected to inhibit electrical current and ion transport at small separations that may be required for x-ray measurements. Cyclic voltammetry measurements indicate that the electrode current does not decrease until the electrode approaches within ~0.5 mm of the window. The typical separation will be larger than 1.5 mm. This cell has been tested in different orientations for satisfactory fluid flow.

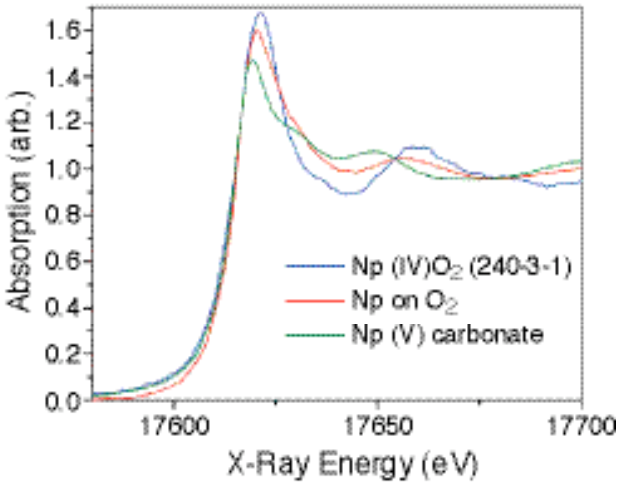

Figure 2. XANES of the Np on the UO_2 surface (red spectrum) and spectra of Np(IV) (blue) and Np(V) (green). Initial pH 6.5.

Natural Sequestration of Radionuclides In Volcanic Tuff

Jonathan Icenhower[1], Edgar Buck[1], Eric Pierce[1], Dawn Wellman[1], and Andreas Lüttge[2]
[1]Pacific Northwest National Laboratory (PNNL) | [2]Rice University

Research Objectives

The cardinal goal of this investigation has been to gain an understanding of the mobility of dissolved elements in a dynamic geochemical environment, in which sequestration of elements may occur due to secondary mineral precipitation. A dynamic geochemical environment is present at the proposed Yucca Mountain repository site, because of the inherent thermodynamic instability of the matrix that is the source of dissolved radionuclide elements—UO_2—and the porous lithologies through which the solution migrates—the volcanic tuff. Previous experimental and modeling studies have shown that pore fluids interacting with volcanic tuff that makes up the bedrock in the disposal setting results in massive displacement of soluble elements in spent nuclear fuel (SNF) and the growth of secondary phases. We studied secondary phase growth and element mobility on the UO_2 surface and in the tuff to form the basis of mechanistic and predictive models. These data will establish source-term and retention parameters, and will underpin a more precise model of radionuclide migration and retention that will refine existing models.

Approach

Because of interruptions in the funding for this work, many of the key experiments are still ongoing and will continue through FY07 and into FY08. Accordingly, what is reported herein is only a fragmentary picture of the complete set of data that we are gathering. The four main thrusts of the experiments are to quantify: (1) the dissolution behavior of the volcanic tuff, (2) the transport of elements through the tuff, (3) the corrosion/dissolution of UO_2 at repository conditions, and (4) the combined dissolution/reaction behavior of UO_2 and volcanic tuff in a single experiment. The dissolution of volcanic tuff and UO_2 was carried out in traditional flow-through experiments over a range of *T*, pH, flow rate, and groundwater compositions. Concentrations of dissolved constituents were determined by inductively coupled plasma–optical emission spectroscopy (ICP–OES) and –mass spectroscopy (–MS) methods, and run products were examined using vertical scanning interferometry (VSI) and atomic force microscopy (AFM). Transport of elements (Ba, Cs, I, Mo, Sr, Se, and Re) was quantified in hydraulically saturated columns. Concentrations of elements from these ongoing experiments that have taken place over the last two years are not yet available. The reaction behavior of UO_2 and volcanic tuff is being determined in a hydraulically unsaturated column (pressurized unsaturated flow, or PUF) test that consists of UO_2 powder overlying tuff powders. The input solution is a synthetic groundwater solution doped with trace amounts of nonradiogenic elements (Ba, Cs, I, Mo, Sr, and Se) or a nonradiogenic substitute (Re for Tc). Effluent solutions are being analyzed using ICP–OES and –MS methods, and run products will be scrutinized by SEM and HRTEM methods. No data are currently available from this experiment.

Accomplishments

Volcanic Tuff Dissolution

Dissolution kinetics of volcanic tuff powders as a function of pH and temperature are shown in Figure 1. Dissolution rates based on Si release to dilute solution at 40° and 90°C

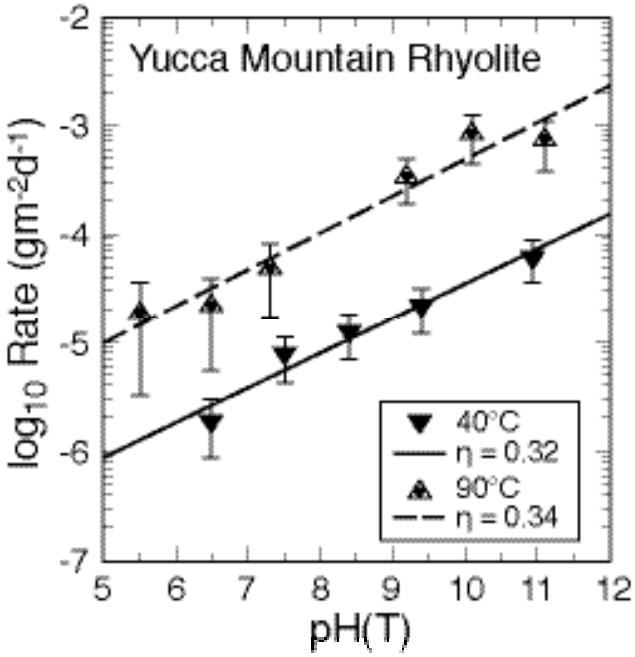

Figure 1. Plot of $\log_{10}$ rate v. solution pH at temperature for Yucca Mountain tuff at 40° and 90°C. The power law coefficient, η, was measured as 0.3 at both temperatures.

indicate a strong dependence on solution pH. The power law coefficient for the rate dependence on dissolution, or the exponent to which the rate is raised, was measured as $\eta = 0.3$ at both temperatures. At high pH values, the effluent chemistry data indicate formation of secondary phases. Run products from experiments with tuff coupons were examined by VSI methods, and a representative image is shown in Figure 2. The figure shows that devitrified matrix—consisting of feldspar and silica polymorphs—dissolves more rapidly than feldspar phenocrysts. Run products were also viewed using AFM, and representative images are shown in Figure 3. These images show the nature of the dissolution surface in the tuff matrix and the formation of nascent secondary phases. A thick reaction layer was not observed in these experiments. These data are included in a manuscript that is being written for the *American Journal of Science*.

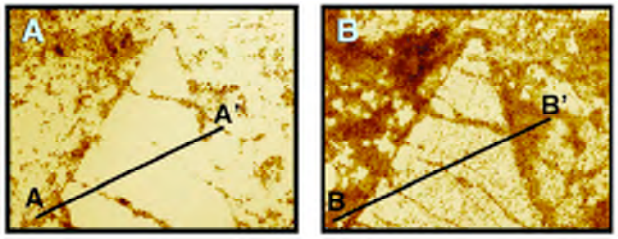

Figure 2. Vertical scanning interferometer (VSI) image of alkali feldspar phenocryst in volcanic tuff matrix before (A) and after (B) dissolution test. The increase in brownish "grunge" in (B) indicates a greater degree of dissolution in the matrix compared to the phenocryst.

Dissolution of UO_2

Although the dissolution behavior of UO_2 has been widely reported in the literature, we were surprised by some of the new surface features that we observed from our experiments. Dissolution experiments were carried out in flow-through reactors at a variety of temperatures and input solution chemistries. We found that once a pH, temperature, and bicarbonate threshold is crossed, dissolution rates rapidly decline. The reason for this is unclear, but it

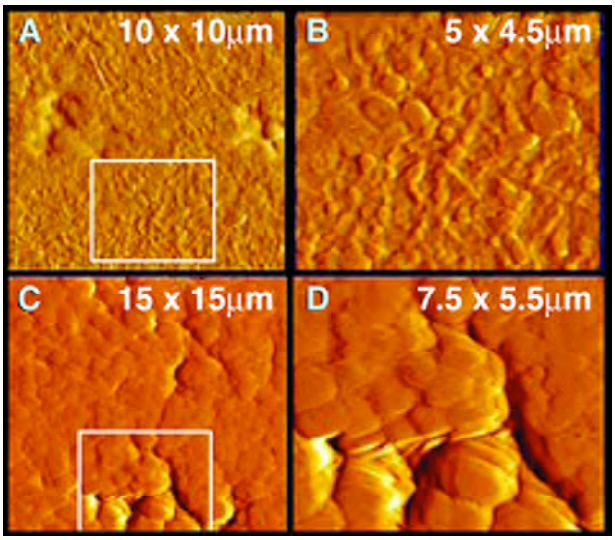

Figure 3. AFM images of volcanic tuff matrix after subjected to dissolution test- the matrix compared to the phenocryst.

appears that a secondary sodium uranyl carbonate mineral forms a continuous film across the UO_2 surface. We are laboring to determine if this result is repeatable and to identify the film on the UO_2 surface. We have a pending manuscript in *Journal of Nuclear Materials* that includes these results.

Transport and reaction mechanisms from UO_2 into volcanic tuff that affect the entire suite of radioactive elements are being determined in detail. If it can be shown that important radioactive elements are less mobile than presently assumed, and that aqueous corrosion rates of SNF (presently assumed to be at the forward rate of reaction) are far slower than current models imply, more realistic source-term and attenuation values can be utilized in repository performance assessments. In addition, a decision to utilize less exotic and expensive engineered barriers, with potential savings of hundreds of millions of dollars, may be supported by newer, more meaningful experimental strategies.

Surface Charge and Radionuclide Adsorption Characteristics of U(IV,VI) Oxyhydroxides at 25–150°C

David J. Wesolowski, Laetitia Delmau, Lawrence M. Anovitz, Jorgen Rosenqvist, and Donald A. Palmer
Oak Ridge National Laboratory (ORNL)

Research Objectives

Uraninite is the primary spent nuclear fuel (SNF) matrix, and until oxidized, it is the surface most likely to come in contact with aqueous solutions that might mobilize radionuclides. The objectives of this project are to determine, in NaCl brines at 25° to 150°C: (a) the pH and temperature dependencies of the proton-induced surface charge density of UO_2 (uraninite); and (b) the sorption affinities of actinide and analog ions on uraninite surfaces. This information can be used to develop surface site complexation models to describe ion adsorption on SNF materials under near-field repository conditions.

Approach

We and our collaborators have pioneered experimental investigations of metal oxide solubility, surface charging and pH-dependent ion adsorption at temperatures ranging from 10° to >250°C, using our unique high-temperature pH-measurement and electrophoresis systems (Wesolowski et al., 2000; Machesky et al., 2001; Zhou et al., 2003; Fedkin et al., 2003). Oxide surfaces are positively charged at pH's below the pH_{pzc} and negatively charged at higher pH. This charge accumulation attracts ions of opposite sign, which adsorb on the surface. We have also developed thermodynamically rigorous surface complexation models (cf. Ridley et al., 2004; 2005) that quantitatively predict the equilibrium adsorption constants of protons, monovalent anions, and mono-, di-, and trivalent cations on metal oxide surfaces to high temperatures. These experimental and modeling approaches enable useful investigation of the sorptive properties of uranium oxide phases found within breached radioactive waste packages at the elevated temperatures predicted in the near-field environment.

Accomplishments

Uraninite Surface Charge and Ion Adsorption at Elevated Temperatures

Nearly stoichiometric uraninite ($UO_{2.08}$) was synthesized by reacting ^{235}U-depleted UO3 in low-density steam at 600°C, with the H_2 partial pressure fixed within the uraninite stability field by the Mn/MnO buffer system, similar to an approach previously used to synthesis pure magnetite (Wesolowski et al., 2000). The point of zero charge of the uraninite powder was determined at 25° and 50°C in 0.1 and 1.0 molal NaCl solutions, using a glass-electrode autotitrator system and data reduction scheme as described by Ridley et al. (2002). The pH of zero net surface charge of this uraninite is shown to be similar to that of rutile (α-TiO_2) over the temperature range studied. Experimental problems were encountered in attempts to

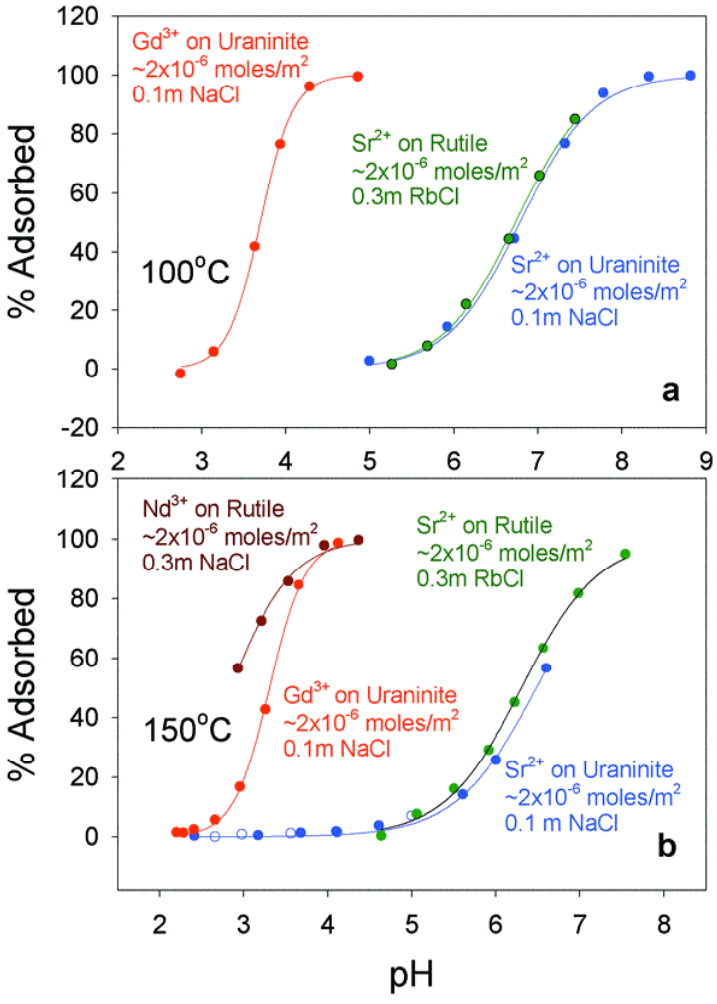

Figure 1. Sorption of Sr^{2+} and Gd^{3+} on uraninite compared with Sr^{2+} and Nd^{3+} adsorption on rutile powder surfaces from pH titrations at 100 and 150°C.

extend the pH_{pzc} to higher temperatures in our hydrogen-electrode pH cells, due presumably to protolytic side-reactions associated with H_2 interaction with the uraninite surface. However, the hydrogen-electrode cells could be used to determine sorption isotherms (Figure 1) for the uptake of nonradioactive analog ions (Sr^{2+}, Gd^{3+}) by uraninite powder surfaces at 100° and 150°C, since these measurements do not require highly-precise proton-balance calculations. As can be seen in Figure 1, the sorption of Sr^{2+} and Gd^{3+} on uraninite is similar to the sorption of Sr^{2+} and Nd^{3+} on rutile powder surfaces, at similar surface loadings and ionic strengths in NaCl solutions.

Actinide and Analog Adsorption on Uraninite at Room Temperature

This series of experiments was designed to measure the adsorption of trace levels (<10^{-5} molal) of radioactive isotopes of Sr^{2+}, Gd^{3+} and Am^{3+} onto the same uraninite powder described above, at 25°C in NaCl solutions. As a comparison, Gd^{3+} sorption on rutile was also measured. A series of aqueous solutions at constant ionic strength (0.03m, NaCl), with calibrated pHs, and containing a known amount of the sorbing ion of interest, were mixed with a carefully weighed amount of uraninite. Results with Sr^{2+} and Gd^{3+} indicated that the adsorption only reached 100% when these elements were originally present in very low concentrations. Otherwise, the sorption isotherms had the expected sigmoidal shape (see Figure 1), but with a plateau lower than 100%. Experiments were conducted with different amounts of uraninite and different concentrations of Sr^{2+} and Gd^{3+}. They all indicated that the uranium oxide surface was saturated at a lower sorbant concentration than expected. Also, the pH at which the adsorption starts appears to be somewhat lower than expected, based on our results obtained using the hydrogen electrode cell. However, the order of the pH values at 50% of adsorption is correct—i.e., 2.83 for Gd^{3+} and 3.05 for Sr^{2+}.

Carrying out these experiments radiometrically allowed the comparison between a trivalent lanthanide (Gd^{3+}) and a trivalent actinide (Am^{3+}). These experiments were done with these elements at trace level (<10-5 molal). Results are presented in Figure 2. Because of the large amount of information already available for adsorption of cations onto rutile, we carried out a series of experiments showing the similarities and differences. Figure 3 presents the results obtained with Gd^{3+}, showing that uraninite and rutile adsorb gadolinium at somewhat different pH values for the same conditions. While the pH for uraninite is lower in both cases, the difference seems to be less when the cation is initially present at concentrations of approximately 10^{-3} molal.

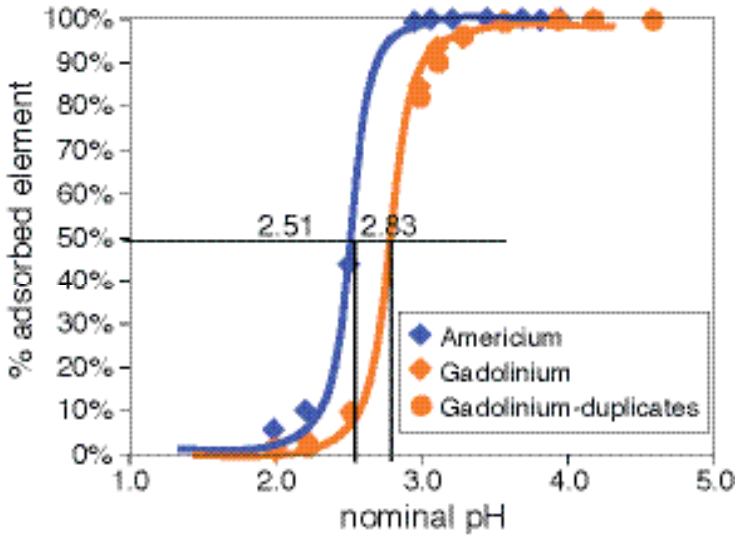

Figure 2. Comparison between Gd and Am adsorption on uranium oxide. Am and Gd are present at trace level, ionic strength of the aqueous phase I = 0.03 m (NaCl).

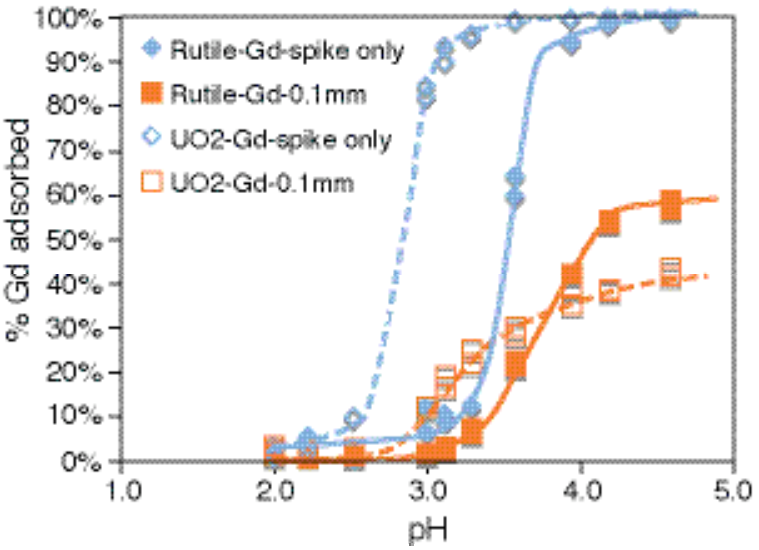

Figure 3. Comparison between Gd^{3+} adsorption on uranium oxide and rutile. Gd^{3+} is present either at trace level or at a concentration of 0.1 millimolal, ionic strength of the aqueous phase I = 0.03 molal (NaCl).

Summary

Despite some experimental difficulties, we have observed that the surface charging and ion (Sr^{2+}, Gd^{3+}, Am^{3+}) adsorption characteristics of near-stoichiometric uraninite ($UO_{2.08}$) are similar to those of rutile (α-TiO_2) in NaCl brines (0.03–1.0 molal) at temperatures of 25° to 150°C. These preliminary results demonstrate that additional studies would be useful in better defining the surface chemistry of uraninite, but that surface charge development and ion sorption characteristics of rutile can probably be used as a surrogate for modeling the interaction of uraninite with dissolved radionuclide cations, until more information is made available on uraninite. This is a very useful finding, since rutile is one of the most widely studied mineral phases, in terms of its surface chemistry and ion adsorption properties, particularly at elevated temperatures in high-chloride brines.

Related Publications

Fedkin, M.V., X.Y. Zhou, J.D. Kubicki, A.V. Bandura, S.N. Lvov, M.L. Machesky, and D.J. Wesolowski, High temperature microelectrophoresis studies of the rutile/aqueous solution interface. Langmuir, 19, 3797–3804, 2003.

Machesky, M.L., D.J. Wesolowski, D.A. Palmer, and M.K. Ridley, On the temperature dependence of intrinsic surface protonation equilibrium constants: An extension of the revised MUSIC model. J. Colloid Interface Sci., 239, 314–327, 2001.

Ridley, M.K., Machesky, M.L., Palmer, D.A. and Wesolowski, D.J., Potentiometric studies of the rutile-water interface: Hydrogen-electrode concentration-cell versus glass-electrode titrations. Colloids and Surfaces A, 204, 295–308, 2002.

Ridley, M.K., Machesky, M.L., Wesolowski, D.J. and Palmer, D.A., Modeling the surface complexation of calcium at the rutile-water interface to 250°C. Geochim. Cosmochim. Acta, 68, 239-251, 2004.

Ridley, M.K., M.L. Machesky, D.J. Wesolowski, and D.A. Palmer, Surface complexation of neodymium at the rutile-water interface: A potentiometric and modeling study in NaCl media to 250°C. Geochim. Cosmochim. Acta, 69, 63–81, 2005.

Wesolowski, D.J., M.L. Machesky, D.A. Palmer, and L.M. Anovitz, Magnetite surface charge studies to 290°C from in situ pH titrations. Chemical Geology 167, 193–229, 2000.

Zhou, X.Y., X.J. Wei, M.V. Fedkin, K.H. Strass, and S.N. Lvov, Zetameter for microelectrophoresis studies of the oxide/water interface at temperatures up to 200°C. Rev. Scientific Instru. 74, 2501–2506, 2003.

This page intentionally left blank.

Waste Form–Waste Package Interactions in the Near Field

In-Package Sequestration of Radionuclides at Yucca Mountain: Waste Package Corrosion Studies Using Small Mockup Experiments
B. Elizabeth Anderson, Katheryn B. Helean, and Patrick V. Brady, Sandia National Laboratories (SNL); Rodney C. Ewing, University of Michigan

In-Package Sequestration of Radionuclides at Yucca Mountain: Neptunium Surface Complexation Subtask
James Jerden, Argonne National Laboratory (ANL)

Uptake of Technetium (Tc) by Iron-Based Materials
Kenneth Krupka, Christopher F. Brown, Steve M. Heald, H. Todd Schaef, Bruce W. Arey, and Michelle M. Valenta, Pacific Northwest National Laboratory (PNNL)

This page intentionally left blank.

In-Package Sequestration of Radionuclides at Yucca Mountain: Waste Package Corrosion Studies Using Small Mockup Experiments

B. Elizabeth Anderson[1], Katheryn B. Helean[1], Patrick V. Brady[1], and Rodney C. Ewing[2]
[1]Sandia National Laboratories (SNL) | [2]University of Michigan

Research Objectives

Knowledge of the corrosion processes and products of spent nuclear fuel (SNF) in a geological repository allows a more thorough understanding of the subsequent release of radionuclides. Corroding A516 steel within the proposed waste packages may create locally reducing conditions, thus changing the likely corrosion products of UO_2, which forms the bulk of SNF. Also, ferrous iron, Fe^{2+}, has been shown to reduce UO_2^{2+} to UO_2(s), and some ferrous iron-bearing ion-exchange materials absorb radionuclides and heavy metal. Therefore, high electron availability of the steel corrosion products may inhibit corrosion of UO_2 and reduce and immobilize problematic species such as TcO_4^-, NpO_2^+, and UO_2^{2+}. The focus of this study is on the nature of Yucca Mountain-relevant steel corrosion products and their effects on local redox state, SNF corrosion, and radionuclide transport.

Approach

Six small-scale (~1:40 by length) waste package mockups were constructed using 316 stainless steel, the same material as the inner layer of the proposed Yucca Mountain waste packages. Twenty-five 1 x 10 x 0.2 cm strips of A-516 carbon steel, the material used as guides for SNF inside proposed waste packages at Yucca Mountain, were inserted into each waste package. The mockups differed with respect to water input, access to the atmosphere, and temperature, and two of the mockups also contain 0.1 g powdered UO_2. Simulated Yucca Mountain process water (YMPW) was injected into the mockups at a rate of 200 µL per day five days a week, using a calibrated needle syringe. The YMPW consists of 50 mg/L silica as sodium metasilicate (and thus, 38.3 mg/L Na), enough HCl to lower the pH to 7.6, and an excess of powdered calcite. The solution was allowed to equilibrate with the atmosphere for an additional five days. The final pH stabilized at 7.5.

Characterization of corrosion products was by x-ray powder diffraction (XRD), scanning electron microscopy (SEM), and, where appropriate, transmission electron microscopy (TEM), x-ray photoelectron spectroscopy (XPS), and sequential leaching for uranium. The ferrous to ferric iron ratio (Fe^{2+}/Fe^{3+}) was measured in the effluent using colorimetry and in the solids using either a standard $K_2Cr_2O_7$ titration (Sandia ASTM D 3872-86) or acid digestion followed by colorimetry. These ratios and measured water pH were input into the geochemical modeling program EQ3/6 to estimate the oxygen fugacity inside of the waste package.

Accomplishments

Although the generally poor crystallinity of the corrosion products precludes reliable quantitative analysis by XRD, major phases were identified in the high-temperature scoping study at 30 and 90 days and in two significantly corroded UO_2-free mockups. The waste package exposed only to humid air showed no significant corrosion after one year. Magnetite, Fe_3O_4, possibly along with the structurally identical but fully oxidized maghemite, was the major corrosion phase present in all cases. The presence of Fe^{2+} was confirmed by wet chemistry. Hematite was identified as a minor phase in the high-temperature scoping study at both 30 and 90 days, and in the 90-day sample a diffraction peak corresponding to a d-spacing of 12.87Å was also evident in x-ray data from the solids. This phase could not be identified from a single XRD peak. However, subsequent SEM with energy dispersive spectroscopy (EDS) on a polished cross section indicates a "fibrous" phase into which Cl is preferentially incorporated, and micrographs suggest a layered structure (Figure 1). A backscattered electron micrograph shows oxidation "blisters" pock-marking the steel surface and clear zones that can be described as anodic (oxidizing) and cathodic (reducing). Solids analysis from the one-year tests are ongoing, but show similar results.

The effluent analysis from both mockup experiments indicate that *in situ* O_2 fugacities were of the order 10^{-36} bar. It is important to note that even after a year of exposure to moist air, the majority of the low alloy steel remained uncorroded and shiny, indicating that anaerobic corrosion is significantly slower than oxidative corrosion processes.

The presence of reduced iron in magnetite in waste package mockup studies suggests not only that radionuclide-sorbing minerals will be present in Yucca Mountain waste packages, but also that the in-package environment will be reducing. This is confirmed by the effluent analyses that

constrain fO_2 to 10^{-36} bar, well below ambient. Hematite is also expected to be present in significant amounts at elevated temperatures, which may be the case at the repository, and possibly also a layered chloride phase. If this layered phase does form in a real waste package, it could be important for the uptake of radionuclides and in maintaining reducing conditions, particularly if it is related to another layered phase, green rust. Ongoing experiments with UO_2 will provide further insight into the effects of steel corrosion on radionuclide transport. This study suggests that steel and its corrosion products may retard transport of U and other radionuclides in Yucca Mountain waste packages and the environment.

Publications

Husler, J.W., B.E. Anderson, K.B. Helean, C.R. Bryan, and P.V. Brady, Ferrozine micro-method for the determination of iron in solids. In preparation, 2007.

Anderson, B.E., K.B. Helean, J.W. Husler, C.R. Bryan, P.V. Brady and R.C. Ewing, Waste package corrosion studies using small mockup experiments. In preparation, 2007.

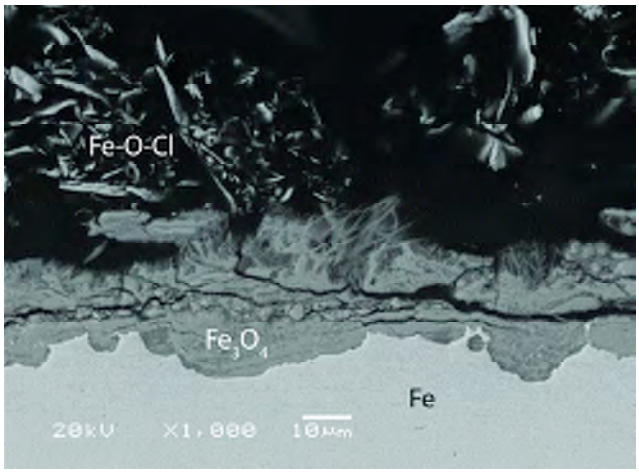

Figure 1. Backscattered electron micrograph of corroded steel in the heated mockup after ninety days. The loosely consolidated fibers, which are consistent with the layered structure noted in the XRD data, are enriched with chlorine relative to the other corrosion products.

In-Package Sequestration of Radionuclides at Yucca Mountain: Neptunium Surface Complexation Subtask

James Jerden
Argonne National Laboratory (ANL)

Research Objectives

This subtask of the Source Term In-Package Sequestration Project had three main objectives: (1) to quantify the distribution of neptunium between common iron oxide minerals [goethite (α-FeOOH), magnetite (Fe_3O_4)] and aqueous solutions as a function of pH, ionic strength, sorbent/sorbate ratio, reaction time (aging), and solution composition; (2) to use synchrotron based x-ray absorption and fluorescence techniques to obtain molecular-scale information (e.g., local coordination environment, oxidation state) on how neptunium is bound to mineral surfaces; and (3) to quantify the reversibility of neptunium sorption onto the iron oxide mineral surfaces. Goethite and magnetite were chosen as sorbents for this study, because they are anticipated to be important corrosion phases within a breached waste package containing steel.

Approach

The sorption experiments were performed in stirred batch reaction vessels. Neptunium-bearing solutions with known pH, ionic strength, and composition were reacted with powders of goethite or magnetite for specific time intervals. Uranium was added to some tests to study possible competition between uranium and neptunium for sorption sites. The vessels were constantly stirred, and contained air filled headspaces that were regularly replenished by opening the vessel and blowing clean air into the bottle before recapping. All solution concentrations were measured by inductively coupled plasma mass spectrometry (ICPMS). Sorbate solutions consisted of either 0.001 molar sodium chloride or a simulated Yucca Mountain pore water. The simulated pore water was a calcite equilibrated, sodium silicate solution containing: 5.0E-3 molal Na^+, 8.0E-4 molal $SiO_2(aq)$, 5.0E-4 molal Ca^{2+}, and approximately 6.0E-3 molal HCO_3^- + CO_3^{2-}. Neptunium-loaded goethite sorbent samples from selected tests were resuspended in the simulated pore-water solution for 21 days to measure neptunium desorption. The pH of the desorption tests was adjusted to approximately 5.8 using HCl. Selected sorbent samples were analyzed by x-ray absorption spectroscopy (XAS) to determine the oxidation state and coordination environment of the adsorbed neptunium. Extended x-ray absorption fine structure (EXAFS) spectroscopy and x-ray absorption near-edge structure (XANES) spectroscopy measurements were made at the Materials Research Collaborative Access Team (MRCAT) 10ID beam line at the Argonne National Laboratory Advanced Photon Source (APS).

Accomplishments

Results from the sorption experiments are shown in Figure 1. Distribution coefficients for neptunium sorption on goethite and magnetite in 0.001 NaCl range from less than 1000 mL/g at low pH to over 10,000 mL/g at pH > 6.5. Distribution coefficients as high as 100,000 mL/g were measured for the sorption test performed in the simulated pore waters. XAS results show that neptunium complexes with the goethite surface as Np(V). The neptunium adsorbed to goethite shows Np-O bond length of approximately 1.8 angstroms, which is representative of the Np-O axial bond in the neptunyl(V) complex. The neptunyl(V) ion is coordinated to 5 or 6 equatorial oxygens with Np-O bond lengths of 2.45 angstroms. The absence of a clearly recognizable Np-Fe interaction for the sodium chloride sorption tests suggests that neptunium in these solutions adsorbs as an outer-sphere complex. XAS results from the calcium-bearing sodium silicate sorption tests show evidence for a neptunyl(V) inner-sphere surface complex with a Np-Fe interaction at 3.5 angstroms and a possible Np-Ca interaction. This possible Np-Ca bond may indicate the presence of neptunium-bearing calcite at the goethite surface. XAS results from the magnetite sorption tests show that both Np(IV) and Np(V) are present on the mineral surface, indicating that some fraction of the Np(V) in solution was reduced to Np(IV) by the magnetite. Desorption tests indicate that samples in which neptunium was bound as inner-sphere complexes show significant sorption hysteresis (greater than 90% of sorbed neptunium was not desorbed).

Our results indicate that under certain conditions, neptunium will be sequestered by waste package corrosion products as tightly bound (not readily desorbed) inner-sphere complexes, or by a co-precipitation process involving the incorporation of neptunium into a carbon-

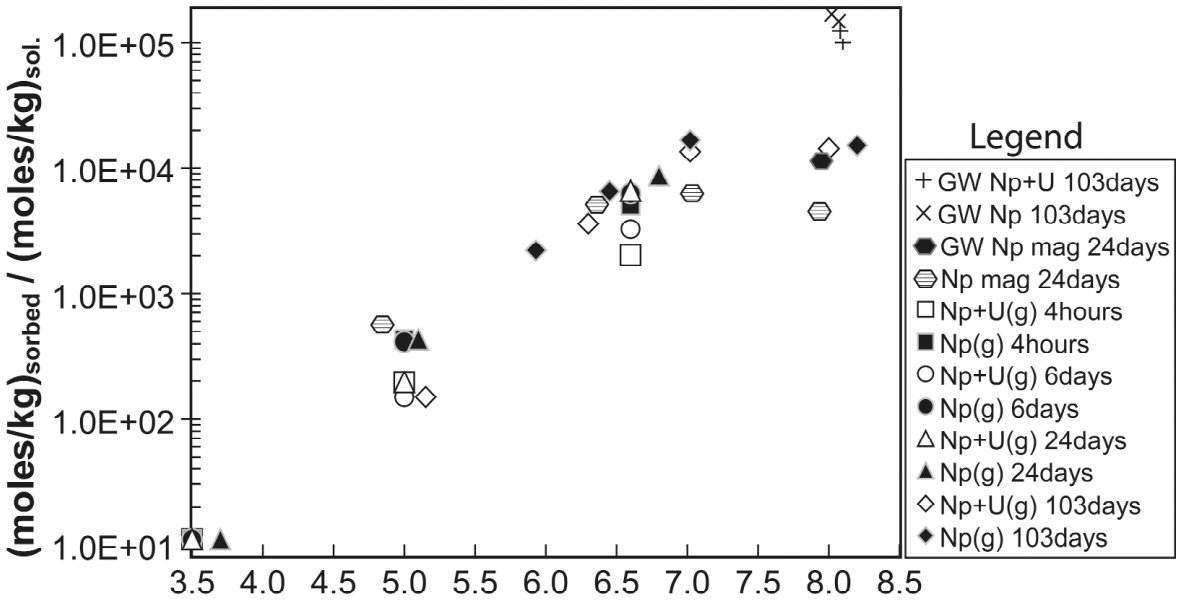

Figure 1. Results from Np sorption tests on goethite showing distribution coefficients for Np sorption (moles of Np adsorbed per kg of sorbent / moles Np per kg of solution in contact with sorbent). The samples labeled GW are from sorption tests performed in simulated groundwater; all other tests were done in ~0.001 molal sodium chloride solutions—(g) denotes goethite sorbent, (mag) denotes magnetite sorbent.

ate mineral. The reduction of neptunium on magnetite could potentially catalyze the precipitation of the sparingly soluble neptunium solid NpO_2. These results represent an important new data set for optimizing surface complexation models for neptunium sorption.

Related Publications

Jerden, J.L, Jr., and A.J. Kropf, Surface complexation of neptunium(V) with goethite. In: Scientific Basis for Nuclear Waste Management XXX, D.S. Dunn, C. Poinssot, and B. Begg, eds. (Mater. Res. Soc. Symp. Proc. 985), Warrendale, PA, 2007.

Jerden, J.L. Jr., J. Kropf, and Y. Tsai, Surface complexation of actinides with iron oxides: implications for radionuclide transport in near-surface aquifers. Eos Trans. AGU, 86(52), Fall Meet. Suppl., Abstract 0800h-H31B-1290, 2005.

Uptake of Technetium (Tc) by Iron-Based Materials

Kenneth M. Krupka, Christopher F. Brown, Steve M. Heald, H. Todd Schaef, Bruce W. Arey, and Michelle M. Valenta
Pacific Northwest National Laboratory (PNNL)

Research Objectives

This work focuses on characterizing the surface-mediated, heterogeneous reduction/sorption reactions that affect the sequestration of ^{99}Tc by Fe oxide/hydroxide solids, which precipitate during corrosion of Fe-based materials used in the waste package, such as A 516 carbon steel used in the fuel basket.

Approach

Batch reaction experiments were used to examine the sorption of dissolved pertechnetate [Tc(VII)] on Fe oxide/hydroxide solids that precipitate during the corrosion of A 516 carbon steel coupons reacted with ^{99}Tc(VII) [0 (blank), 0.001, 0.1, and 1.0 mmol/L] spiked simulated Yucca Mountain pore water or dilute water (i.e., undersaturated with respect to carbonate). Test vials were sacrificed and sampled at various time points. The resulting solutions were analyzed potentiometrically for pH and by inductively coupled plasma-optical emission spectroscopy (ICP-OES) for the concentrations of major cations and some trace metals. Concentrations of other trace metals and ^{99}Tc were measured by inductively coupled plasma-mass spectrometry (ICP-MS). Bulk x-ray diffraction (XRD) and scanning electron microscopy (SEM), in conjunction with energy dispersive spectroscopy (EDS), were used to characterize the unreacted and corroded steel coupons and Fe corrosion products, as well as to determine the location of sorbed ^{99}Tc. Synchrotron-based x-ray analyses, including x-ray microfluorescence (μXRF), x-ray absorption near-edge structure (XANES), extended x-ray absorption fine structure (EXAFS), and x-ray microdiffraction (μXRD), were used to determine the speciation and redox state of ^{99}Tc incorporated Fe oxides present on the corroded carbon steel coupons.

Accomplishments

Results of the ^{99}Tc studies suggest that ^{99}Tc would sorb during the formation of steel corrosion products, and would, during this process, be reduced from ^{99}Tc(VII) to the sparingly soluble ^{99}Tc(IV) oxidation state. As a result of this surface-mediated, heterogeneous reduction/sorption process, the inventory of ^{99}Tc released from breached waste packages would be expected to be lower than what is now conservatively estimated.

Earlier results from similar batch reaction experiments and characterization studies conducted with dissolved perrhenate [Re(VII)], as a surrogate for ^{99}Tc(VII), are presented in Krupka et al. (2006a,b). Although the Re experiments also demonstrated that Re would sorb with Fe oxides/hydroxides that precipitate during the corrosion of steel, the XANES and EXAFS analyses indicated, unlike the results from the ^{99}Tc studies, that Re was not reduced from the +7 to the +4 oxidation state during this reaction, as originally expected (Krupka et al., 2006a,b). The results from the Re and ^{99}Tc studies suggest that the standard potential for the Re(VII)/Re(IV) redox couple may be significantly lower than that for the ^{99}Tc(VII)/^{99}Tc(IV) couple. Thus, Re may not be an adequate surrogate for studying the geochemical behavior of ^{99}Tc at environmentally relevant reducing conditions.

The solution analyses from the ^{99}Tc experiments and direct characterization of the steel coupons contacted by both ^{99}Tc-spiked solution matrices, using SEM/EDS and synchrotron-based x ray analyses, confirmed the uptake of ^{99}Tc(VII) during the formation of steel corrosion products. Less corrosion had occurred in the experiments spiked with ^{99}Tc(VII) compared to those spiked with Re(VII). The extent of corrosion in the ^{99}Tc(VII) experiments also decreased with increasing concentrations of dissolved ^{99}Tc(VII), especially at 1.0 mmol/L ^{99}Tc(VII). These results are consistent with results of other studies that show pertechnetate [^{99}Tc(VII)] to be effective at inhibiting the corrosion of iron and steel (Cartledge, 1966). Additionally, the amount of corrosion on the coupons reacted with simulated pore water versus those reacted with dilute water was considerably less after 175 days of reaction time. XRD results for the corroded steel coupons and the filter samples showed that the corrosion products consisted primarily of magnetite (Fe_3O_4) and lepidocrocite [γ-FeO(OH)], sometimes goethite [α-FeO(OH)], and possibly maghemite (γ-Fe_2O_3). SEM/EDS analyses of the corrosion products on the reacted coupons revealed the presence of ^{99}Tc in the corrosion product (Figure 1). Because the reacted coupons were rinsed several times with their respective ^{99}Tc free starting solutions prior to storage and solid-phase characterization, the ^{99}Tc associated with the corrosion products is

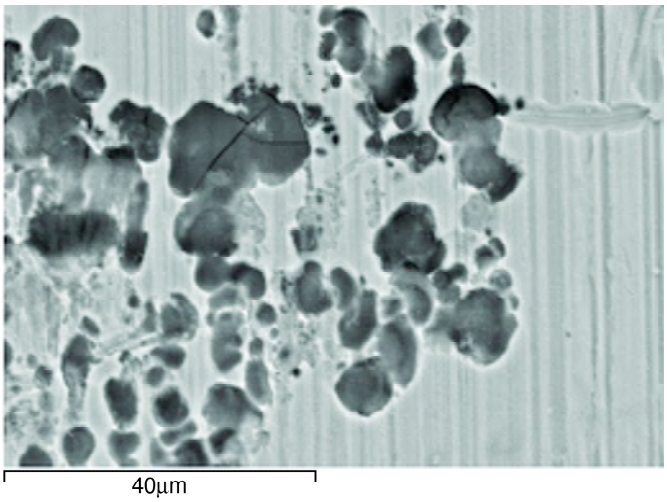

Figure 1. SEM micrograph of typical corrosion pits (dark areas) that formed after 175 days on the A 516 carbon steel coupons reacted in 0.1 mmol/L ^{99}Tc(VII)-spiked simulated pore water. (EDS identified the presence of Tc in these corrosion pits.)

currently assumed to be co-precipitated with the corrosion product, rather than surface adsorbed. XANES analyses of ^{99}Tc present on the reacted coupons show that >80% of the sorbed ^{99}Tc was reduced from the +7 to +4 oxidation state upon incorporation into the Fe corrosion products (Figure 2). The EXAFS data were fit by a

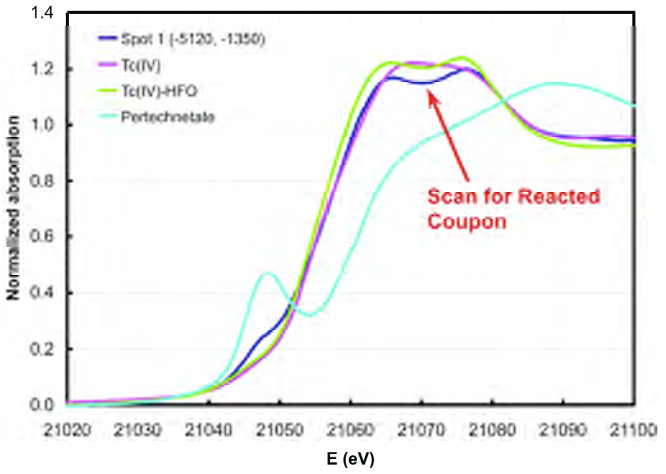

Figure 2. ^{99}Tc near edge data (dark blue) for a typical spot on corroded coupon reacted in dilute water spiked with 0.1-mmol/L dissolved ^{99}Tc(VII) compared to spectra for ^{99}Tc(VII) (light blue) and ^{99}Tc(IV) (green and pink spectra) standards.

linear combination of the spectra for 99TcVIIO_4^- and ^{99}TcIV-HFO (amorphous hydrous Fe(III) oxide) standards. A preliminary evaluation indicates that the EXAFS had a better fit using the ^{99}Tc-HFO standard (Zachara et al., 2007) for ^{99}Tc(IV) rather than hydrated ^{99}TcIVO_2 solid. These results indicate that the sorbed ^{99}Tc(IV) is in an octahedral environment, sharing an edge with a single neighboring Fe-O octahedron.

The Pacific Northwest National Laboratory is operated by Battelle for the U.S. Department of Energy under Contract DE-AC05-76RLO 1830. The synchrotron-based x-ray analyses were completed at the Advanced Photon Source (APS) beamlines 20 BM and 20 ID (PNC-CAT) at the Argonne National Laboratory. Use of APS is supported by the DOE Office of Science, Office of Basic Energy Sciences, under Contract No. W-31-109-Eng-38.

References

Cartledge, G. H., The passivation of iron in the presence of pertechnetate and chromate ions. Journal of the Electrochemical Society, 113, 328–333, 1966.

Krupka, K.M., C.F. Brown, H.T. Schaef, S.M. Heald, M.M. Valenta, and B.W. Arey, Rhenium uptake as analogue for ^{99}-Tc by steel corrosion products. In: Proceedings of the 11th International High-Level Radioactive Waste Management Conference (IHLRWM), April 30–May 4, 2006, Las Vegas, pp. 905–912, American Nuclear Society, La Grange Park, IL, 2006a.

Krupka, K.M., C.F. Brown, M.M. Valenta, H.T. Schaef, and B.W. Arey, Uptake of technetium (Tc) by iron-based materials. In: Office of Science and Technology and International (OST&I) Annual Report 2005, pp. 43–44, DOE/RW-0581, U.S. Department of Energy, Office of Civilian Radioactive Waste Management, Washington, DC, 2006b.

Zachara, J.M., S.M. Heald, B.-H. Jeon, R.K. Kukkadapu, C. Liu, J.P. McKinley, A.C. Dohnalkova, and D.A. Moore, Reduction of pertechnetate [Tc(VII)] by aqueous Fe(II) and the nature of solid phase redox products. Geochimica et Cosmochimica Acta, 71, 2137–2157, 2007.

Integration of In-Package Chemical and Physical Processes

Computational Studies on the Corrosion of Spent Nuclear Fuel and the Adsorption and Incorporation of Radioactive Elements into Mineral Phases
Udo Becker, University of Michigan

A Model for Radionuclide Release from Spent Nuclear Fuel
Carl I. Steefel, John Apps, Nicolas Spycher, and Eric Sonnenthal, Lawrence Berkeley National Laboratory (LBNL)

This page intentionally left blank.

Computational Studies on the Corrosion of Spent Nuclear Fuel and the Adsorption and Incorporation of Radioactive Elements into Mineral Phases

Udo Becker
University of Michigan

Research Objectives

Reaction mechanisms and the thermodynamics of incorporating radioactive elements on minerals and secondary phases during the alteration of waste products often cannot be adequately investigated using experimental or field approaches. However, quantum mechanical computational approaches can often help in determining reaction pathways, as well as the thermodynamics and kinetics of corrosion processes and mobilization (and re-immobilization) of radioactive elements in the environment of nuclear waste repositories. Computational approaches allow us to study the oxidation mechanism of spent nuclear fuel (SNF) and the role of water and temperature in the corrosion process. The atomic, electronic, and spin structure of the bulk material and specific surfaces are evaluated, and the thermodynamics of the adsorption of radioactive complexes are calculated as a function of adsorbing mineral and specific surface features (such as steps, kinks, and defect sites). In all of these reactions, electron transfer and, thus, potential redox mechanisms are monitored. Finally, computational studies are often the only tool that can investigate whether radioactive elements can be incorporated into mineral phases or corrosion products. Structural changes can be analyzed together with the energy of substitution, which is an important measure of the amount and long-term fate of radionuclides in their host phases.

Approach

At present, we have three graduate students involved in these projects: Frances N. Skomurski (OCRWM Fellowship), Lindsay Shuller (OCRWM Fellowship), and Elizabeth Anderson (OCRWM Fellowship; NSF Fellowship). In our research group, we have focused our efforts in three research areas: (1) The corrosion of UO_2 in dry and wet environments, associated transition states, and their influence on the long-term stability of SNF; (2) the incorporation of Np into U^{6+} alteration phases as a possible long-term sink for this radioactive element; and (3) the adsorption and redox behavior of Tc complexes on mineral surfaces.

Accomplishments

The Corrosion of UO_2

The initial corrosion of UO_2 was studied computationally in dry and wet conditions. While water makes adsorption of oxygen thermodynamically more stable, more important is its influence on the energy lowering of activated complexes upon O_2 approach. Water dramatically increases the adsorption kinetics from ~1000 years for the oxidation of one monolayer of UO_2 in dry conditions to immediate oxidation of UO_2 in a wet atmosphere.

Np Incorporation into U^{6+} Alteration Phases

Understanding the behavior of Np is important, because Np is a potential contributor to long-term dose due to the half-life of Np-237 of ~2.1 million years, and because Np^{5+} is mobile as neptunyl complexes. This study uses quantum-mechanical calculations to determine the most energetically favorable Np-incorporation mechanism into studtite, $[UO_2O_2(H_2O)_2](H_2O)_2$, and boltwoodite, $HK(UO_2)(SiO_4)(H_2O)_{1.5}$. For studtite, we compare Np^{5+}-incorporation (Equation 1; here $Np^{5+} \leftrightarrow U^{6+}$ substitution is charge-balanced by the addition of H+) to Np^{6+}-incorporation (Equation 2).

$$[UO_2O_2(H_2O)_2](H_2O)_2 + NpF \rightarrow [(U,Np)O_2O_2(H_2O)_2](H_2O)_2 + UF_6 \quad (1)$$

$$[UO_2O_2(H_2O)_2](H_2O)_2 + 1/2Np_2O_5 \rightarrow [(U,Np)O_2O_2(H_2O)_2](H_2O)_2 + UO_3 \quad (2)$$

While Equation (1) preserves oxidation states of all elements and results in a low substitution energy (0.93 eV), the hexafluoride reference phases are not expected to play a major role in a repository environment. Equation (2) requires the correct modeling of spin ordering in Np_2O_5. In addition to the mechanism in Equations 1+2, Np^{5+} incorporation has been evaluated, requiring optimization of additional H^+ ions in different locations. For this latter case, the lowest incorporation energy found so far is 4.57 eV, which is too high for studtite to be considered a major Np sink.

Boltwoodite, a uranyl sheet silicate with Na^+/K^+ ($+H_2O$) interlayer cations, is a common alteration phase observed in SNF dissolution studies. Np^{5+} incorporation for U^{6+} was tested, and the system was charge-balanced by adding H^+ (Figure 1) in different locations, by replacing K+ in the

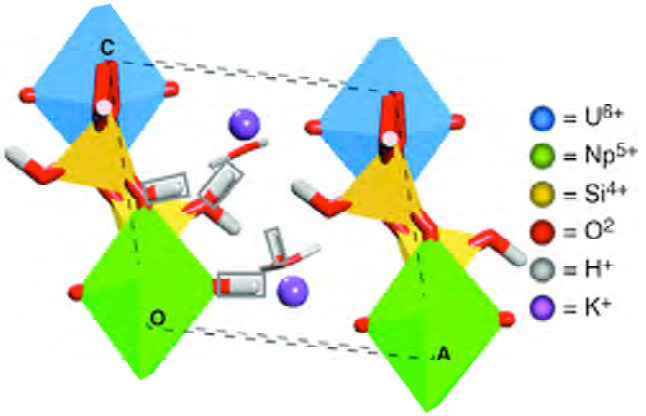

Figure 1. Np^{5+} incorporated into the boltwoodite structure with all the possible H^+ positions labeled with a box around the H^+ atom.

interlayer by Ca^{2+}, or Si^{4+} by P^{5+}. The first two substitution mechanisms result in substitution energies of ~1.4 eV. Due to the unit cell size of the reference phases (feldspars), a mixture of quantum mechanical (uranyl phases) and experimental thermodynamic data (feldspars) were used for these calculations.

Tc and Re Adsorption/Reduction onto Different Mineral Phases

Technetium is of interest because its radioactivity and high mobility as pertechnetate (TcO_4^-) suggest it being a major contributor to long-term dose on release from a nuclear waste repository. ReO_4^- is often used as a chemical analogue for TcO_4^-, which is justified by the elements' similar radii and major oxidation states of +7 and +4, as well as their similar ranges over Eh-pH space of TcO_4^- and ReO_4^-. However, this analogy may fail in a variety of conditions—conditions being tested in this study.

A series of batch sorption experiments allows a more direct comparison between the elements adsorbed to a suite of nine redox-sensitive materials: hematite, galena, pyrite, goethite, magnetite, Fe^0, hydroxyapatite doped with 10% Fe, sphalerite, and pyrrhotite. Relative adsorption are compared by measuring the remaining ReO_4^- or TcO_4^- in solution and oxidation states of Re or Tc in the solids. Batch experiments performed using Re in air resulted in measurable uptake only by Fe.

As a complement to these tests, optimized geometries, adsorption energies, and electronic structures of Tc and Re complexes on galena clusters are calculated quantum-mechanically, including changes in hydration energies. These calculations show that the adsorption of TcO_4^- to a galena terrace is similar to that of ReO_4^- in both energy and geometry. Two potentially stable geometries were found for adsorption to step edges (Figure 2). For the second configuration, we observe a reduction of the anions from total charge of -1 to -2, indicating a transfer of one electron from the galena cluster to pertechnetate or perrhenate. This position is favorable for TcO_4^- but unfavorable for ReO_4^-, suggesting that TcO_4^- will be reduced by galena step edges, but ReO_4^- will not.

References

Anderson, B.E., U. Becker, K.B. Helean, and R.C. Ewing, Perrhenate and pertechnetate behavior on iron and sulfur-bearing compounds. Proceedings of the Materials Research Society, 985 (in press), D.S. Dunn, C. Poinssot, and B. Begg, eds., 2007.

Shuller, L.C., R.C. Ewing and U. Becker, Np-incorporation into uranyl phases: A quantum-mechanical approach. Proceedings of the Materials Research Society, 985 (in press), D.S. Dunn, C. Poinssot, and B. Begg, eds., 2007.

Skomurski, F.N., R.C. Ewing, A.L. Rohl, J.D. Gale, and U. Becker, Quantum mechanical vs. empirical potential modeling of uranium dioxide (UO_2) surfaces: (111), (110), and (100). American Mineralogist, 91, 1761–1772, 2006.

Skomurski, F.N., L.C. Shuller, R.C. Ewing, and U. Becker, The corrosion of UO_2 versus ThO_2 and the role of electron transfer. Journal of Nuclear Materials (submitted), 2007.

Skomurski, F.N., U. Becker, and R.C. Ewing, Computational investigation of the formation of hyperstoichiometric uranium dioxide (UO_{2+x}). Proceedings of the Materials Research Society, 985 (in press), D.S. Dunn, C. Poinssot, and B. Begg, eds., 2007.

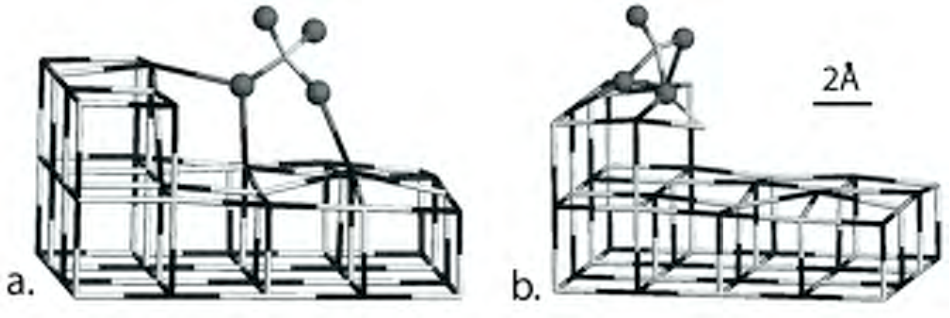

Figure 2. Two possible final positions for TcO_4^- and ReO_4^- are a galena step edge. ReO_4^- prefers position (a), while TcO_4^- prefers position (b).

A Model for Radionuclide Release from Spent Nuclear Fuel

Carl I. Steefel, John Apps, Nicolas Spycher, and Eric Sonnenthal
Lawrence Berkeley National Laboratory (LBNL)

Research Objectives

The primary objective of this project was to develop conceptual and numerical models for the prediction of the progressive release of radionuclides from a breached spent nuclear fuel (SNF) container when exposed to seepage and condensate water. The model incorporates the partial oxidation and dissolution of uranium oxide, the precipitation of alteration products, the solid solution substitution and/or adsorption of other actinides (e.g., Np, Pu, and Am) during precipitation of the secondary uranyl phases, radionuclide decay, and alpha particle and gamma radiation on aqueous phase radiolysis. The SNF model is then coupled to thermal-hydrologic-chemical (THC) processes occurring in the near field and drift environment, including O_2 and CO_2 transport and flow and evaporation of seepage water, so as to provide a more realistic description of the total environment within which SNF degradation occurs.

Approach

The technical approach reflects the current conceptualization of a hypothetical waste package failure, in which ingress of either seepage water or condensate leads to contact with SNF along cladding cracks. The environment may be fully saturated (liquid only), or (more likely) may include a gas phase in which relatively rapid transport of the reactive gas species O_2 and CO_2 can occur. Given this physical setting, the principal focus was on developing a kinetic model for the degradation of U(IV) oxides and the subsequent precipitation of a variety of secondary U(VI) phases according to the Ostwald Rule of Stages (Steefel and Van Cappellen, 1990). The kinetic treatment of the Ostwald Rule of Stages was found to be necessary to capture the rapid release of uranium over short time scales (~1–2 years), followed by a much lower uranium flux as more stable U(VI) oxide phases come to dominate with time (Wronkiewicz et al., 1992).

Accomplishments

In order to develop a validated numerical model, drip tests conducted at 90°C at Argonne National Laboratory, using uranium oxide wafers (summarized by Wronkiewicz et al., 1992), were simulated (Figure 1).

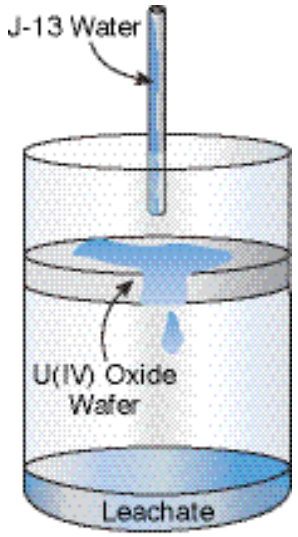

Figure 1. Schematic illustration of Argonne drip tests with U(IV) oxide wafers (Wronkiewicz et al, 1992) that were used for model validation.

The SNCF degradation was considered to take place by the oxidative dissolution of uraninite (UO_2) coupled to the precipitation of a soluble precursor-phase schoepite ($UO_3{\cdot}2H_20$), followed by the growth of more stable becquerelite ($CaU_6O_{19}{\cdot}10H_2O$) on the schoepite mineral surface over time. The kinetic rate laws considered include the precipitation of schoepite without a nucleation barrier, according to

$$R_{Schoepite} = -A_{Schoepite} k \left(1 - Q/K_{eq}\right),$$

where R is the rate, A is the surface area of the schoepite, k is the rate constant, Q is the ion activity product, and Keq is the equilibrium constant. This is followed by the irreversible growth of becquerelite on the schoepite surface:

$$R_{Becquerelite} = -A_{Schoepite} k_{Ostwald}.$$

According to this model, the nucleation of becquerelite is inhibited, and the mineral can only form by effectively cannibalizing the schoepite surface. As the mass of the more-stable-phase becquerelite increases with time, its rate

of formation eventually becomes dominated by growth on its own surface, according to

$$R_{Becquerelite} = -A_{Becquerelite} k \left(1 - Q/K_{eq}\right).$$

Simply decreasing the rate of precipitation of becquerelite by a small amount leads to a very-short-term suppression of its formation (days), while a larger decrease leads to its complete suppression altogether. Simple manipulation of the rate constants for becquerelite therefore cannot produce a match of the observations in the Argonne drip tests, and a kinetic model incorporating the Ostwald Rule of Stages along the lines of the formulation presented above is necessary. The results are summarized in Figure 2.

This Ostwald Rule of Stages model developed here and implemented in the code CrunchFlow captures the approximately 1-year period in which only schoepite was observed in the Argonne drip tests, followed by the appearance of becquerelite and other stable phases in Year 2 and 3. The model also captures the early high flux of uranium, followed by a lower flux once the more stable uranium phases come to dominate the solution chemistry (Figure 3).

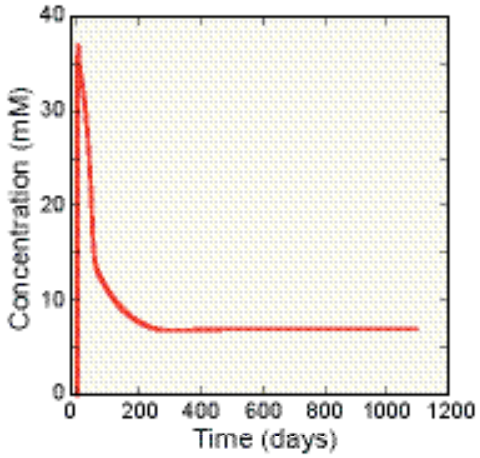

Figure 2. Ostwald Rule of Stages model for the formation of the more stable becquerelite using schoepite as a precursor. With generation of sufficient becquerelite surface area, crystal growth dominates and the solution chemistry is controlled by this phase.

Publications

Steefel, C.I., J.A.Apps, and N. Spycher, A kinetic model for the Ostwald Rule of Stages with application to the oxidative dissolution of uraninite (in preparation).

References

Steefel, C.I., and P. Van Cappellen, A new kinetic approach to modeling water-rock interaction: The role of nucleation, precursors, and Ostwald ripening. Geochmicia et Cosmochimica Acta, 54, 2657–2677, 1990.

Wronkiewicz, D.J., J.K. Bates, T.J. Gerding, E. Veleckis, and B.S. Tani, Uranium release and secondary phase formation during unsaturated testing of UO_2 at 90°C. Journal of Nuclear Materials, 190, 107–112, 1992.

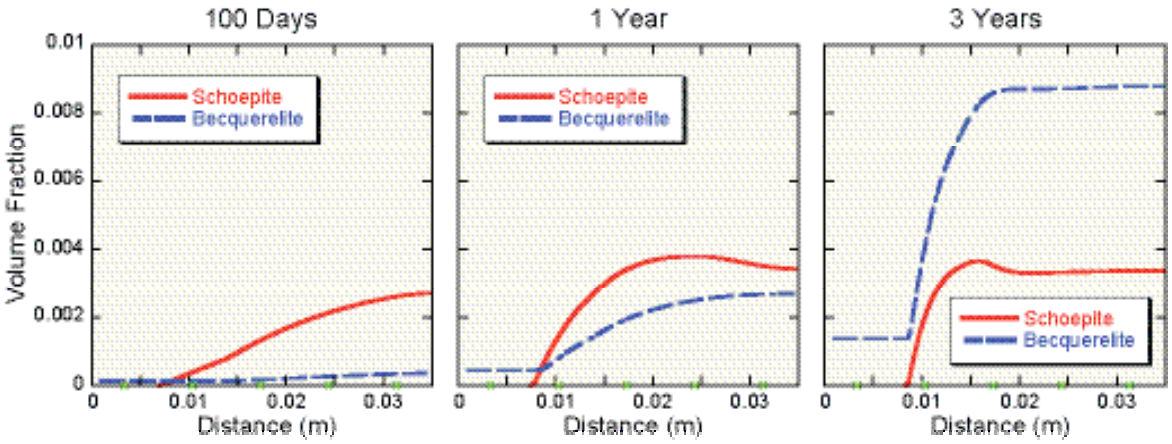

Figure 3. Simulated early release of uranium while schoepite dominates the solution chemistry, followed by a lower uranium flux once the more stable becquerelite develops enough reactive surface area that it can dominate kinetically.

This page intentionally left blank.